ESD Pub. 4881

QUANTIFYING DIFFUSIVE MASS TRANSFER IN FRACTURED SHALEBEDROCK

P.M. Jardine[1*], W.E. Sanford[2], J.P. Gwo[3], O.C. Reedy[1], D.S. Hicks[1], J.S. Riggs[4], and W.B. Bailey[1]

[1]Environmental Sciences Division, Oak Ridge National Laboratory, Oak Ridge, Tennessee
[2]Department of Earth Resources, Colorado State University, Fort Collins, Colorado
[3]Center for Computational Sciences, Oak Ridge National Laboratory, Oak Ridge, Tennessee
[4]Instruments and Control Division, Oak Ridge National Laboratory, Oak Ridge, Tennessee

* Corresponding author

ABSTRACT

A significant limitation in defining remediation needs at contaminated sites often results from an insufficient understanding of the transport processes that control contaminant migration. The objectives of this research were to help resolve this dilemma by providing an improved understanding of contaminant transport processes in highly structured, heterogeneous subsurface environments that are complicated by fracture flow and matrix diffusion. Our approach involved a unique long-term, steady-state natural gradient injection of multiple tracers with different diffusion coefficients (Br, He, Ne) into a fracture zone of a contaminated shale bedrock. The spatial and temporal distribution of the tracers was monitored for 550 d using an array of groundwater sampling wells instrumented within a fast flowing fracture regime and a slow flowing matrix regime. The tracers were transported preferentially along strike-parallel fractures, with a significant portion of the tracer plumes migrating slowly into the bedrock matrix. Movement into the matrix was controlled by concentration gradients established between preferential flow paths and the adjacent rock matrix. Observed differences in tracer mobility into the matrix were found to be a function of their free-water molecular diffusion coefficients. The multiple tracer technique confirmed that matrix diffusion was a significant process that contributed to the overall physical nonequilibrium that controlled contaminant transport in the shale bedrock. The experimental observations were consistent with numerical simulations of the multi-tracer breakthrough curves using a simple fracture flow model. The simulated results also demonstrated the significance of contaminant diffusion into the bedrock matrix. The multiple tracer technique and ability to monitor the fracture and matrix regimes, provided the necessary experimental constraints for the

accurate numerical quantification of the diffusive mass transfer process. The experimental and numerical results of the tracer study were also consistent with indigenous contaminant discharge concentrations within the fracture and matrix regimes of the field site. These findings suggest that the secondary source contribution of the bedrock matrix to the total off-site transport of contaminants is relatively large and potentially long-lived.

INTRODUCTION

A vast accumulation of literature in the fields of soil science, geosciences, and petroleum engineering has provided overwhelming evidence that solute transport in undisturbed subsurface media is often influenced by preferential flow coupled with matrix diffusion (Shuford et al., 1977; Shaffer et al., 1979; Frohne and Mercer, 1984; Abelin et al., 1987, 1991; Seyfried and Rao, 1987; Jardine et al., 1988, 1990, 1993a; Birgersson and Neretnieks, 1990; Wilson et al., 1993; McKay et al., 1993a; Schettler and Parmely, 1993; Novakowski and Lapcevic, 1994; Vandergraaf et al., 1996; Holtta et al., 1996; Reedy et al., 1996; Selim and Ma, 1998). The physical structure of most subsurface media is conducive to rapid advective flow along fractures, cracks, inter-aggregate regions, root channels, and animal burrows. As a result, concentration and hydraulic gradients develop between the advective flow paths and the surrounding soil and bedrock matrix which causes time-dependent mass exchange between the two domains. The occurrence of this physical nonequilibrium process in soils was evidenced more than a century ago (Schumacher, 1864; Lawes et al., 1882); however, the challenge remains on how to quantify this process in soils and bedrock for the purpose of aiding (a) nutrient use efficiency in crops and trees (Shuford et al., 1977; Shaffer et al., 1979; Haines et al., 1982; Jardine et al., 1989; Wilson et al., 1991a,b), (b) oil,

gas, and resource recovery (Frohne and Mercer, 1984; Schettler and Parmely, 1993; Khire and Khan, 1994 a,b), (c) waste management strategies (Walter, 1982; Abelin et al., 1987; Cacas et al., 1990 a,b; Neretnieks, 1993; Birgerson et al., 1993), and (d) remediation of contaminated environments (Ahn et al., 1985; Solomon et al., 1992; Wilson et al., 1993; Jardine et al., 1993 a,b; Shevenell et al., 1994; Gwo et al., 1996; Moline et al., 1998).

A number of techniques are available for assessing physical nonequilibrium processes during solute transport in heterogeneous subsurface environments (Jardine et al., 1998). The techniques include (1) controlling flow path dynamics with manipulations of pore-water flux and soil-water tension, (2) isolating diffusion processes with flow interruption, (3) using tracers that visually map flow path dynamics, (4) using tracers with different diffusion coefficients, and (5) using multiple tracers with grossly different sizes. At the field scale, techniques (4) and (5) are most practical for quantifying advective preferential flow and time-dependent diffusion into the soil and bedrock matrix (Albelin et al., 1987; Harvey et al., 1989, 1993, 1995; Raven et al., 1988; Maloszewski and Zuber, 1990, 1993; McKay et al., 1993 a,b, 1995; Sanford and Solomon, 1998; Jaynes and Horton, 1998).

The use of multiple tracers with different diffusion coefficients is particularly useful since the influence of matrix diffusion on the overall system dispersion can be quantified. When physical nonequilibrium processes are significant in subsurface media, tracers with larger molecular diffusion coefficients will be preferentially "lost" to the matrix porosity relative to tracers with smaller molecular diffusion coefficients. Abelin et al. (1987) noted that the effective diffusivities

of various conservative dye tracers were smaller than I^- during transport in fractured granite. This was believed to be the result of matrix diffusion effects since the dye tracers were larger molecules relative to I^-. Similarly, Birgersson and Neretnieks (1990) found that I^- diffused farther into the matrix of the same granitic material relative to Uranine and Cr(III)EDTA which is consistent with the larger diffusion coefficient of I^- relative to the other two tracers. Likewise, Vandergraaf et al. (1996) observed that the conservative tracer ^{131}I eluted considerably later than Uranine in a quarried granite block containing natural fractures. Although not mentioned by the authors, the separation of the tracer breakthroughs could have resulted from diffusion into the rock matrix although diffusion rates into granite are small. Maloszewski and Zuber (1990, 1993) suggested that double tracing should be applied as a rule in order to confirm the significance of matrix diffusion and to distinguish the apparent dispersion from the intrinsic one. These authors have reworked several field experimental data sets (e.g. Garnier et al., 1985; Raven et al., 1988; Cacas et al., 1990b), where multiple tracers were used in fractured chalk and gneiss bedrock to show that diffusion into the matrix was the dominant process controlling solute transport. Recently, Sanford and Solomon (1998) used the noble gas tracers He and Ne to quantify matrix diffusion in a fractured weathered shale saprolite containing a large microporosity. The separation of the gas breakthrough curves was consistent with differences in the tracer molecular diffusion coefficients.

From the perspective of contaminant transport, solute mobility into the matrix creates a secondary contaminant source that drastically alters the choice of remediation strategies by severely limiting the usefulness of various techniques. For this reason, deciphering the mechanisms of field-scale contaminant transport processes is imperative to successful risk assessment and decision-making

concerning site remediation. Model sensitivity analysis of contaminant transport has suggested that the movement of mass between fracture and matrix domains is one of the most important variables in describing solute mobility in heterogeneous subsurface systems (Neretnieks, 1980; Berglund and Cvetkovic, 1995; Toran et al., 1995; Brogan and Gailey, 1995). Unfortunately, this area of research is lacking in experimental data, particularly in fractured bedrock.

In this study, we adopted a multiple tracer technique to quantify the significance of fracture flow and matrix diffusion on the fate and transport of contaminants in fractured shale bedrock at the Oak Ridge National Laboratory. Our goal was to provide an improved understanding and predictive capability of field scale diffusion mechanisms for the purpose of enhancing the selection of remedial strategies at contaminated sites. Our objective was to demonstrate that the fractured shale bedrock not only acts as a conduit for contaminants, but that it also serves to "attenuate" contaminants via diffusion into the higher porosity rock matrix. To fulfill this objective, a unique experimental approach was necessary that involved a long-term, near steady-state natural gradient injection of multiple tracers and the ability to monitor the bedrock fracture and matrix regimes over time. Coupling the two techniques proved to be invaluable for quantifying diffusive mass transfer in the shale bedrock.

MATERIALS AND METHODS

Site Description and Rationale

The study site is located in the southeast portion of Waste Area Grouping 5 (WAG 5) on the Oak Ridge Reservation in Oak Ridge, Tennessee (Fig. 1). It is situated in the Valley and Ridge

Province, which is characterized by a succession of northeast-trending thrust faults that duplicate the Paleozoic age sedimentary rock sequences. Locally, the site is underlain by the Dismal Gap formation which consists of interbedded shale - limestone sequences that dip 30-35° southeast. The site is situated in the upper unit of the Dismal Gap, which has a greater proportion of shale and therefore a greater number of fractures and hydrologically active zones. Most fractures within the upper bedrock are only a few centimeters to a meter in length, but they are numerous and highly interconnected (Solomon et al., 1992). Bedding plane fractures are also prevalent within the bedrock and they are typically more continuous (Lee et al., 1992). Fracture densities fall within the range of approximately 200/m found in overlying saprolites (Dreier et al., 1987), and 5/m measured in fresh rock (Sledz and Huff, 198 1; Lemiski, ORNL, 1996, unpublished data).

Our investigations focused on shallow groundwater flow within saturated bedrock 2-9 m below the ground surface and below the bedrock-saprolite interface. The site is near the valley floor where converging groundwater flows west to east along geologic strike toward a cross-cutting tributary drainageway. Fracture orientations and connectivity can give rise to extensive preferential flow regimes within the bedrock.

Our rationale for choosing this site is based on monitoring evidence that showed this area was a significant contributor to the total off-site transport of tritium (Wickliff et al., 1991; Hicks et al., 1992). Disposal records confirm that the southeast portion of WAG 5 contains hundreds of unconfined shallow land burial trenches where ^{3}H has been disposed. Discharge concentrations from a seep at the bottom of the site were 20,000 times higher than the safe drinking water

standard. Likewise, a survey of ^3H concentrations in evapotranspired water, conducted in the southeast portion of WAG 5 above hundreds of waste trenches, revealed elevated levels of ^3H across the entire area (Wickliff et al., 1991). More significant was the fact that the highest activities were found near the end of two long trenches that were strike parallel with the seep 35 m away. These observations were the basis behind our hypothesis, that fracture orientation and converging groundwater flow paths contribute to the massive flux of contaminants being discharged from waste sources to surface water systems on the Oak Ridge Reservation. Our challenge was to quantify the advective movement of these contaminants and verify whether secondary sources are forming in the bedrock matrix due to solute diffusion.

Site Installation and Tracer Injection Strategies

In order to understand the mechanisms of contaminant discharge at this site, as well as similar sites that are complicated by heterogeneous multi-region flow, we initiated a multiple tracer experiment that required well installations within different flow regimes of the bedrock.

Borehole installation, characterization, and sampling setup

We initially drilled three boreholes at locations aligned parallel to strike, forming a transect between the seep and the waste trenches containing elevated ^3H concentrations (Fig. 1). The boreholes were approximately 1.6, 7.6, and 18.4 m from the buried waste trench boundary (wells 4014, 4165, and 2046, respectively). For each borehole, the upper 2-3 m of saprolite was augured, and a 10.2 cm drive casing was pushed in place before the remainder of the hole was drilled. A double-tube core barrel was used with tap water in wet rotary coring to produce a 7.6

cm diameter hole that was 7 to 9 m deep. Core samples were collected during this process and they revealed a highly fractured interbedded shale - limestone bedrock.

A borehole video camera was used to examine the formation characteristics in-situ. As described by Moline et al. (1998), the camera allowed for visualization of the boreholes and identification of discrete fracture zones; however, it was not possible to identify which fractures were flowing. The camera did reveal that most of the formation is significantly fractured and that a discrete zone towards the middle of each well contained a structurally incompetent section of bedrock. We would later learn that this zone was a highly fractured groundwater conduit (1-2 m long in vertical distance) that was susceptible to collapse.

A borehole dilution, or point-dilution method was used to estimate the average specific discharge of groundwater in the formation as a function of depth (Halevy et al., 1967; Drost et al., 1968; Hicks et al., 1992; Sanford and Moore, 1994; and Novakowski et al., 1995). Specific discharge measurements suggested that a rapid flowing interval was present at 232.5 to 234.3 m above mean sea level (amsl) within the bedrock (Fig. 2). The groundwater flux within this region was as high as 300 to 500 m y^{-1} suggesting that it was fractured. The fast flowing fracture regime was surrounded by a slower flowing matrix regime that had observed discharge values significantly less than those of the fractured region. These results corroborate observations of the borehole video camera and visual inspection of rock cores taken from the borehole.

The borehole dilution technique identified rapid and slow flowing regimes within the formation. These results were used to strategically place multilevel solution samplers at a variety of depths within two of the boreholes that were 7.6 and 18.4 m from the trench boundary (wells 4165 and 2046, respectively). The borehole at 1.6 m (well 4014) was used as our tracer injection well (Fig. 2). Solinst® multilevel sampling ports were isolated by 0.46 m long gel-filled pressure packers, providing a sampling interval of 0.3 m. Well 2046 was instrumented with 5 sampling ports and well 4165 was instrumented with 4 sampling ports. A lesser number of ports was used in well 4165 because partial collapse of the borehole, following point-dilution measurements, filled the lower meter of the well with rock debris. The gel-filled packers were expanded with a constant pressurized water head. Solution sampling from each port used low-volume 1/16" ID polyethylene tubing, and dissolved gas sampling at each port used 3/8" ID polyethylene tubing. The design of the sampling apparatus was such that neither sampling protocol affected the other.

Drive-point well installation

Drive-point well installation provided a more rapid and economical means of capturing the spatial and temporal distribution of tracers and contaminants. Most of the 24 drive-point wells were placed within a few meters of the sampling transect that followed strike (Figs. 3 and 4). There were two reasons for this: (1) we wanted to optimize sampling intensity along strike with limited resources, and (2) within 10 m on either side of the transect, the surface soils were heavily contaminated with ^{90}Sr. This latter circumstance would have significantly increased the cost of well installation. The depth to which drive-point wells were installed did not always agree with our expectations. Often, drive-point refusal by the bedrock resulted in shallower than anticipated

samplers (Fig. 4). Nevertheless, we were still able to instrument drive-point wells within the different flow regimes of the formation. Well installation involved hydraulically pushing standard AQ high carbon steel coring rods with a drive-point head into the ground using a novel track-mounted pneumatic hammer design which was capable of penetrating shale bedrock. The groundwater sampling interval for each well was 0.3 m in length and used 18 cm ID slotted pvc tubing.

Injection well installation and tracer injection strategies

Borehole dilution measurements suggested that a rapid flowing fractured zone was present in the bedrock at 232.5 to 234.3 m amsl which was the preferred depth interval for tracer release within well 40 14. Borehole collapse at ~233.3 m amsl in well 40 14 resulted in a less than optimal injection interval of 233.5 to 234.3 m amsl, which is about 2 times smaller than our original intention. The compromised injection interval was plugged at the bottom using bentonite pellets and a single straddle packer, maintained at 500 psi N_2, was used to isolate the injection interval within the fracture regime. Three nonreactive tracers (He, Ne, and Br) which have different molecular diffusion coefficients (i.e., He = 6.0×10^{-4} m^2/d, Ne = 3.5×10^{-4} m^2/d, Br = 2.0×10^{-4} m^2/d) were added to the injection interval as a steady-state pulse for 180 d under natural gradient conditions. The noble gas tracers were added to the groundwater via passive diffusion as described by Sanford et al. (1996). Bromide was added as an aqueous solution of $MgBr_2 \bullet 6H_2O$. A computational datalogger (Campbell Scientific) was used to automatically deliver small increments of a 0.1 mol L^{-1} stock $MgBr_2 \bullet 6H_2O$ solution through a solenoid valve in order to maintain an injection interval concentration of 0.0145 mol L^{-1} Br^- (1159 μg Br^- mL^{-1}). The fluid in

the injection interval was continuously mixed by recirculating groundwater through a Cole Palmer peristaltic pump and flow-thru conductivity probe with temperature compensation. Copper refrigeration tubing was used for the entire circulation system except for a 15 cm long piece of silicon tubing needed in the pump head. The pump rate was set to mix the entire injection interval within 5 min. Flow through the conductivity probe served to trigger the automated addition of Br^- when the conductivity within the injection interval fell below the target value. Conductivity was checked every second and if Br^- was needed the solenoid valve was opened for approximately 14 sec to dispense the Br^- stock solution from a constant head marriotte device at a rate of 0.18 L h^{-1}. The addition of Br^- had a negligible affect on the total volume of the injection interval and this was confirmed with continuous pressure head measurements within the interval.

Groundwater flow through the injection interval was quite steady throughout the injection experiment since the mass of Br^- tracer added was similar from day to day. In fact, the average specific discharge of groundwater through the injection interval based on the rate of Br^- added each day for 180d was calculated to be 248 m y^{-1}, which is similar to an earlier single point-dilution measurement of 300 m y^{-1} (Fig. 2).

Sampling, Monitoring, and Analytical Methods

On October 18, 1994, a natural gradient injection of the three conservative tracers, He, Ne, and Br was initiated. The tracers were injected for 180 d, followed by 370 d of additional monitoring. Because the site was in a remote location, power was supplied with batteries that were charged with over 100 sq. ft. of solar panels. During the winter months, injection line freeze-ups were

prevented with 100 watt light bulbs and insulation. The spatial and temporal variability of the tracers and the contaminant ^3H were monitored during the 550 d period using two multilevel sampling wells, containing a total of 9 sampling ports, and 24 drive-point wells at varying depth (Figs. 3 and 4). Groundwater levels were also measured in the drive point wells at least once a week, with the frequency increasing during storm events. Continuous pressure-head measurements were also performed at several locations throughout the site. The average site horizontal hydraulic gradient was 0.06-0.1 and remained nearly uniform in space and time for the duration of the experiment. A slight rise in the hydraulic gradient occurred over a several month period during conditions of high rainfall and low evapotranspiration (i.e. days 90-140).

Passive in-situ headspace samplers, as described in Sanford et al. (1996), were used to monitor He and Ne transport at the field site. A designated sampler was used in each drive point well and the source well. The concentration of dissolved gases was quantified using gas chromatography. Since our experiment was conducted at a contaminated site with high levels of ^3H, the decay of ^3H to He was a consideration. Groundwater samples indicated that background concentrations of He were negligible and below our lower detection limit.

Groundwater samples were acquired from each well, including the injection well, for analysis of Br^- and ^3H. One well volume was purged from each drive-point well prior to sample collection where the volume varied between 0.1 and 0.5 L. This provided a real time sample and replenished the well with new groundwater that equilibrated with the gas samplers. For the multilevel and source wells, each sample line was purged prior to sample collection where the

volume varied between 0.03 to 0.1 L. Concentrations of Br^- below 5 $\mu g\ mL^{-1}$ were analyzed using ion chromatography, and concentrations greater than 5 $\mu g\ Br^-\ mL^{-1}$ were analyzed with a bromide ion specific electrode. Samples above 5 $\mu g\ Br^-\ mL^{-1}$ that were analyzed using both techniques were in excellent agreement. Tritium analysis was initially performed on samples that were distilled and condensed to remove potential interferences from ^{90}Sr activity (EPA, 1980). It was found that ^{3}H concentrations were so high relative to ^{90}Sr that direct counting of groundwater samples was sufficient. Tritium was analyzed on a TRI-CARB Liquid Scintillation Analyzer, Model 2000CA, Packard Instrument Company.

Photographs of the field facility and a brief overview of this study can be found at http://www.esd.ornl.gov/facilities/hydrology/WAG5/ which was last updated 1/98.

Tracer Plume Contours, Center of Mass, and Plume Velocity Calculations

Bromide concentration contours were generated at specific times using the observed experimental data. Semivariograms of Br^- concentrations were calculated and overlain by a spherical or exponential model. The resultant model parameters were relatively insensitive to whether a spherical or exponential model was used. The model parameters obtained, were then used in kriging within the software Surface III$^+$ (Kansas Geological Survey, www.kgs.ukans.edu, last updated 1/8/98) to generate the resultant Br^- concentration grids that were used for plotting concentration contours. The sparsity of raw data sometimes created exaggerated spreading and observed multimodal concentration distributions within the contours (see Fig. 6). Nevertheless, the tracer concentrations were used to estimate the center of mass in the x and z directions, the

average plume velocity with time, and the total tracer mass at specific locations as a function of time. The computation was performed for times after the tracer injection was terminated and used equations 1-4 in Freyberg (1986). The major sources of uncertainty in these computations are (1) the sparsity of raw data and (2) no prior knowledge of the field-scale medium porosity distribution which is necessary to calculate tracer mass. The field-scale porosity distribution is a heterogeneous field estimated by calibrating a two-region, dual-permeability dual-porosity model against the measured Br^- concentrations. Dual-permeability and dual-porosity imply that both the fracture zone and the matrix zone have matrix and fracture domains, with the total porosity partitioned distinctly between the two domains (Gwo et al., 1995, 1998). The vertical extent of dispersion was assumed to end roughly 1 m below the bottom of wells 4165 and 2046. This assumption is justified by limited mobility of Br^- within the bedrock interval at 2046-E (Table 1). The tracer center of mass can only be calculated to ~270 d because significant Br^- mass begins to exit the field site into the cross-cutting tributary after that time.

RESULTS AND DISCUSSION

Significance of Fracture Flow

Tracer breakthrough in the various wells showed a clear distinction between the fracture regime and the matrix regime, and the results were, for the most part, consistent with the findings of the point dilution tests. Monitoring wells located within the fracture regime typically experienced rapid first arrival times and higher peak tracer concentrations relative to monitoring wells located within the matrix regime (e.g. Table 1). This was consistent with the observation that monitoring wells located within the fractured regime could not be pumped dry with rates as high as 1200 ml

min^{-1}, whereas wells situated within the matrix regime could be pumped dry with rates as low as 200 ml min^{-1}. Tracer breakthrough coupled with point dilution results and well purge rates allowed for an estimate of the approximate fracture and matrix zones (Fig. 4). The distinction between the matrix and fracture regimes is not truly a horizontal plane as depicted in figure 4, but most likely meanders downgradient. A good example of this is well 16, which is shown to reside in the matrix regime (Fig. 4); however, experimental data suggest otherwise. Due to the sparse nature of the monitoring wells, the visual representation of the two distinct flow zones can only be approximated. As indicated in table 1, not all wells were situated within the tracer plume. This was primarily because they were (1) at great distances from the fracture regime into the matrix (wells 4 and 5), (2) upgradient of the source well (wells 1, 2, 3), or (3) down dip from the primary strike-parallel flow field (wells 11, 12, 13, 18b). For ease of discussion and representation, the Br^- tracer results, rather than the dissolved gases, will be used to demonstrate the significance of fracture flow in these systems.

The breakthrough of Br^- within the fracture regime of the shale bedrock showed characteristic plume spreading at greater distances from the source (Fig. 5). Within the fast flowing fracture regime, the solute breakthrough was characterized by a rapid concentration increase followed by a steady-state tracer flux until the pulse was terminated at 180 d (Fig. 5). These results suggest that Br^- was preferentially transported along strike-parallel fractures which is consistent with the conceptual framework of water and solute mobility in these fractured systems (Solomon et al., 1992). The decrease in Br^- concentration 6 m from the source during the period of -100 to 140 d was the result of dilution arising from an increase flux of groundwater through this portion of the

fracture interval. The increased flux resulted from a slowly rising site hydraulic gradient (e.g. 0.06 to 0.1) in response to large rainfall inputs and low evapotranspiration. Recent site investigations have used dissolved oxygen measurements to confirm that the increase in groundwater flux is the result of recent storm water that has infiltrated the upgradient groundwater source (most likely in waste trenches that reside directly above the bedrock).

Horizontal and transverse spreading of the Br^- tracer plume was also evidenced within the fracture intervals. The upward spreading of the tracer plume was the result of slow solute migration into the bedrock matrix (see next section), whereas the downward spreading of the tracer plume most likely resulted from solute migration into a fracture interval that was ~3 times larger than the tracer injection interval (see Materials and Methods, Injection Well Installation). The effect of tracer density on the downward spreading cannot be entirely ruled out even though the density of the groundwater interval with and without tracer was measured to be 1.013 g cm^{-3}. Ronen et al. (1995) have shown tracer density differences as small as 0.0001 g cm^{-3} can cause density induced flow. Strike dominated transport coupled with transverse spreading can best be seen using two-dimensional Br^- concentration contours, generated along the transect of monitoring wells (Fig. 6). The Br^- concentration contours were generated at specific times using the observed experimental data and should be viewed as an approximation of the true concentration field since the sparsity of raw data causes exaggerated spreading near the source (e.g. Fig. 6, 77d) and multimodal concentration distributions farther from the source. Nevertheless, the contours are effective at showing preferential tracer movement along strike and the spreading of tracer upward into the matrix. They also show a time sequence of tracer movement which is useful in defining the

direction of tracer mobility, and where sufficient data exist, the contours allow for estimates on the velocity of the plume center of mass and an estimate of the total mass contribution of tracer within the fracture and matrix regime (see next section).

Since preferential solute mobility along strike was a dominant process controlling tracer migration, a large majority of the Br^- tracer plume was captured within the thin 2-dimensional transect of wells (Fig. 3). Approximately 70% of the injected Br^- tracer mass was accounted for within the narrow cluster of wells 6-10 and 4165 A-D at 6 m from the source, and 60% of the mass was accounted for between wells 17b and 2046 A-E at 17 m from the source (Figs. 3 and 4). These results show the dominance of transverse vertical spreading versus lateral spreading of the tracer plume.

The Br^- results from well 2046 appear inconsistent with several point dilution measurements at this well (Table 1 and Fig. 6 versus Fig. 2), with the latter showing small specific discharge values and the tracer data showing consistently rapid and large breakthrough concentrations. This apparent paradox could be caused by the fact that the two techniques may not have measured the exact same interval, with the point dilution technique potentially sealing off fractures that were included in the tracer study. Also, the point dilution technique provides an average specific discharge for a bedrock interval. If the fracture porosity is very small relative to the packed volume, then it is possible to greatly underpredict the fracture flux by averaging across the entire interval. Therefore, tracer techniques can provide a more realistic indication of the contaminant flux within a bedrock interval.

Significance of Matrix Diffusion

Single tracer intervretation

Although Br^- was preferentially transported along strike parallel fractures, a significant amount of tracer mass was transferred to the bedrock matrix as a function of time (for example Figs. 7 and 8, Table 1). At 6 m from the source, the arrival of significant Br^- tracer <0. 1, 0.8, and 1.4 m into the matrix was 3, 50, and 10 1 d, respectively (Fig. 7). The slow migration of Br^- into the bedrock matrix was most likely driven by concentration gradients between the fracture regime and the matrix regime. It is important to note, that if we had not performed a long-term, steady-state, natural gradient injection, we probably would never have observed tracer migration into the matrix. The long-term injection strategy is synonymous with the long-term leaching of contaminants from waste trenches and subsequent mobility into the surrounding shale bedrock. A traditional short-term forced gradient approach would not have conveyed the same observations, and the important process of solute migration into the matrix would have been missed.

Bromide center of mass and plume velocity calculations also suggested the significance of preferential fracture flow coupled with possible matrix diffusion in this system. As shown in figure 6, the Br^- plume moved preferentially along strike with an average pore water velocity of 47 m y^{-1} and a standard deviation of 38 m y^{-1}. Horizontal spreading, as a result of preferential flow along strike, dominated the movement of mass; however, upward vertical spreading into the matrix was evident. The calculated pore water velocity reflects the effects of rapid solute migration along strike parallel fractures and the slow vertical migration of solutes into the matrix. The variability of this value may arise from several factors including, variations in hydrologic

conditions over the duration of the experiment, the sparse pattern of wells, and the calculated heterogeneous porosity field. Nevertheless, the calculated pore water velocity was similar to center of mass migration rates calculated by Sanford and Solomon (1996) for He and Ne mobility in a weathered shale saprolite. The significance of solute migration into the matrix was further evidenced by calculating total Br^- mass as a function of time in the fracture and matrix regimes. This calculation was possible between 6-9 m from the source because of sufficient monitoring locations within both the matrix and fracture regimes. The results indicated a steady increase in total Br^- mass within the matrix which gradually surpassed the Br^- fracture mass at ~ 60 d (not shown). Over the course of the 180d injection, 30% more Br^- mass was affiliated with the matrix regime relative to the fracture regime. Thus, more solute mass can be expected to reside within the shale matrix if there is a continuous source such as is the case in our experimental design. The implications of these findings are significant from a contaminant transport perspective since thousands of waste trenches on the Oak Ridge Reservation have been continuously leaking contaminants into the subsurface for several decades.

It can be surmised that molecular diffusion is the rate limiting process controlling tracer migration into the matrix since Br^- concentrations generally decreased exponentially with greater distances into the matrix (Figure 7). The one-dimensional fracture flow model, CRAFLUSH (Sudicky and Frind, 1982), was used to simulate Br^- migration within the fracture and matrix regime along the entire transect of sampling wells. Our intentions were not to rigorously model all of the processes contributing to solute migration in this system, but rather to test the hypothesis that diffusion may be controlling the migration of tracer into the matrix. Further, only the ascending limbs of the Br

breakthrough curves were simulated since the model assumes complete recovery of mass from the matrix upon tracer washout, and this was not observed over the time frame of our experiment. The washout portion of the Br^- breakthrough curves show a rapid concentration decrease with extended tailing at very low concentration to long time periods. This is due to slow release of Br^- from the matrix and is consistent with the observed asymmetric breakthrough of tracers in structured media (Seyfried and Rao, 1987; Jardine et al., 1993a; Gwo et al., 1998). Full mass recoveries of Br^- from the matrix would require significantly longer time periods than those studied here. The slow release of Br^- from the matrix is consistent with the mechanism of diffusion and it is this very premise that hampers remediation efforts of contaminated sites in structured media.

Model input parameters were based on independent field and laboratory observations that used subsurface media similar to that at the WAG 5 field facility (Dreier et al., 1987, Wilson et al., 1992; McKay et al., 1995; Dorsch et al., 1996). The mean pore water velocity (v) of the fracture regime was estimated from measured field-scale advective flow rates in fractured saprolite using bacteriophage (McKay et al., 1995). Porosity (θ) was obtained from direct measurements on similar subsurface material (Wilson et al., 1992; Dorsch et al., 1996), and fracture spacing (2B) and aperture (2b) were estimated from measured values in shale bedrock on an adjacent field site (Dreier et al., 1987). Our most significant unknown was the solute travel distance from the fracture regime to the various sampling wells within the matrix regime (z). Observed distances based on measured well depths are subject to large errors since it is impossible to know where the fracture regime ends and the matrix regime begins throughout the site. A good example of this is

well 16 whose depth would imply that it resides within the matrix regime (Fig. 4), yet experimental data suggest otherwise. Therefore, simulations of Br^- transport throughout the entire site involved holding all model parameters constant except the distance into the matrix z. Values of z were varied until an adequate simulation of the observed Br^- movement into the matrix was achieved (for example Fig. 9a). The magnitude of model simulated z values were on average 47% of the measured z values across the entire site. Simulations of Br^- mobility in the matrix regime, simultaneously generate simulations of Br^- transport in the fracture regime (z=0). It is therefore possible to check the adequacy of the model for describing tracer mobility at the field facility since we experimentally measure tracer within both the fracture and matrix regimes. Matching the model to observed Br^- mobility within the matrix, produced reasonable simulations of Br^- transport through the fracture regime (Fig. 9b). This finding suggests that the model, to a certain extent, is accurately describing tracer mobility through the shale bedrock and that diffusion may be an important mechanism in the storage of solutes, particularly contaminants in the shale bedrock. However, the mechanism of diffusion remains uncertain at his point, since it is inferred from modeling results and observations of a single tracer.

Multiple tracer intervretation

A more rigorous test of diffusion-limited mass transfer can be derived from the multiple tracers that were simultaneously injected during the course of our experiment. Besides Br^-, the dissolved gases He and Ne were also continuously injected as a steady-state pulse for 180 d within the fractured regime of the shale bedrock. The three tracers are all nonreactive and differ only in their free water molecular diffusion coefficient, (D_w), where D_w for He is 1.7 times and 3 times larger

than the D_w for Ne and Br, respectively (i.e., He = 6.0 X 10^{-4} m^2/d, Ne = 3.5 X 10^{-4} m^2/d, Br = 2.0 X 10^{-4} m^2/d). All three tracers migrated preferentially along strike, and their concentrations in the fracture regime quickly reached a similar steady-state relative concentration for conditions near the source (i.e., 6-9 m), with the average reduced Ne concentrations somewhat higher than the other two tracers (Fig. 10). Similar steady-state tracer concentrations reflect the short solute residence times within the fracture regime near the source. However, if in fact there was preferential mobility into the matrix of one tracer versus another, we would expect to see a separation of tracer breakthrough at early times during the ascending limb of the breakthrough curve. Unfortunately, the sparsity of noble gas data during this period precludes this analysis (Fig. 10). Since all three tracers had a similar steady-state reduced concentration in the fracture regime, the concentration gradient established between the matrix and fracture regimes would be the same for all three tracers. Thus, for conditions close to the source, observed differences in tracer breakthrough into the matrix would solely be a function of their molecular diffusion coefficients.

The breakthrough of the tracers 6 m from the source and 0.8 m into the matrix relative to the fracture is shown in Figure 11 a. The movement of He and Ne into and out of the matrix was more rapid than Br^-, and this is consistent with the larger molecular diffusion coefficient of the dissolved gases relative to Br^-. However, He concentrations are similiar to, or lag slightly behind those of Ne, even though the diffusion coefficient for He is larger than that for Ne. The reason for this may be the result of slightly higher Ne concentrations in the fracture regime relative to Br^- and He (Fig. 10) which would result in a larger Ne concentration gradient between the two

regimes and thus enhance its migration into the matrix. Similar results were noted for distances 0.1 and 1.4 m into the matrix at 6m from the source (not shown). The separation of the dissolved gas tracer breakthrough concentrations from those for Br^- suggest that matrix diffusion may be contributing to the overall physical nonequilibrium process that controls contaminant transport in the shale bedrock (Maloszewski and Zuber, 1993).

At greater distances from the source, the contributions of matrix interactions were still prominent, and tracer breakthrough profiles remained suggestive of a diffusion mechanism, although at first glance this may not be apparent (Fig. 11 b, c). At 13 m from the source and 0.4 m into the matrix, the breakthrough of the three tracers was nearly simultaneous, with the concentration of gas tracers eventually surpassing Br^- (Fig. 11 b). This was followed by tracer washout after the input pulse was terminated at 180 d. At 23 m from the source and 0.1 m into the matrix, the arrival of Br^- into the matrix was actually earlier than that of the noble gas tracers, which is exactly opposite of what was observed 6 m from the source. This apparent paradox is believed to be caused by the preferential loss of gas tracers to the bedrock matrix closer to the source, as supported by subsequent modeling (see below). Since their was no direct measure of all three tracers in the fracture regime beyond 9 m, we hypothesized that Br^- remained within the advective flow field (fracture regime) for a longer time period, allowing it to be transported greater distances relative to the gas tracers. Having been transported farther down gradient, Br^- experienced the first opportunity to begin diffusing into the matrix at distances further from the source. Eventually, He and Ne arrived at the same locations and also began to diffuse into the matrix, lagging behind that of Br^- (Figs. 11 b,c). Because of the faster diffusion rate of the noble

gases, the movement of He and Ne into the matrix was more rapid, and when given enough time, the He and Ne breakthrough curves eventually surpass the Br^- breakthrough curves (see Fig. 11 b as an example).

At 31 m from the source, the separation of three tracers was even more dramatic (not shown) and followed the same trends observed in Figure 11 c. These results show that solute diffusion into the bedrock matrix is a significant process contributing to contaminant storage in this subsurface media, and that the diffusion process becomes increasingly important as the residence time of the solute increases in the system.

The migration of the three tracers into the bedrock matrix was reasonably well described using CRAFLUSH (Fig. 12). All model parameters were held constant as described earlier and z was matched to the observed Br breakthrough. The only model parameter that differed between the three tracers was their free-water molecular diffusion coefficient (D_w). Model results showed that for conditions close to the source, the migration of Br^- into the matrix was slower relative to the gas tracers, and the migration of Ne was slower than that of He (Fig. 12 a). These results are partially consistent with the observed data since the tracer diffusion coefficients follow He > Ne > Br. Observed He data, however, is far removed from the model simulated curve for reasons unknown to the authors. With increasing distance from the source, model simulated curves more adequately described the observed migration of the three tracers into the matrix (Fig. 12 b,c). At 13 m from the source, model simulated curves merged in a similar manner as the observed data (Fig. 12 b). Further, the simulated curves reproduced the observed early arrival of Br^- into the

matrix followed by He and then Ne. For conditions far from the source (i.e., 23 m), model results again matched the observed tracer concentration trends and showed that Br^- migrated into the matrix ahead of the He and Ne, with Ne migrating more rapidly than He (Fig. 12 c). Numerical confirmation of the observed multi-tracer breakthrough trends, further supports the mechanism of diffusion as an important process controlling the fate and transport of solutes in this shale bedrock. The multiple tracer technique and ability to monitor both the fracture and matrix regimes provided the necessary experimental constraints for the accurate numerical quantification of the diffusion process.

Relation to Indigenous Contaminant Distributions

The experimental and numerical results of the tracer study were consistent with contaminant discharge concentrations within the matrix and fracture regimes at the WAG 5 field facility. As an investigation of opportunity, tritium (^3H) was analyzed in groundwater samples acquired for tracer analysis. Tritium concentrations in monitoring wells located within the fracture regime were consistently lower than ^3H concentrations within the matrix regime. The yearly average ^3H concentration in the fractured regime was ~ 120 μCi L^{-1}, with the concentration of ^3H increasing to as high as 280 μCi L^{-1} within the matrix. Although the concentration of ^3H in the fractured regime was consistently lower than the concentration of ^3H in the bedrock matrix, the mass flux of ^3H migrating through the fractures was nearly 10 times greater than that moving through the matrix. Nevertheless, a significant ^3H concentration gradient exists between the fracture and matrix regimes of the experimental field facility (e.g. Fig. 13). The direction of the contaminant

concentration gradient is opposite the experimental tracer gradient, suggesting that the primary contaminant source feeding the fracture regime has diminished over the years, and contaminants stored in the matrix over the past several decades are diffusing back into the fracture regime. Figure 13 shows seasonal groundwater ^3H concentration profiles within the fracture and matrix regimes 7.6 m from the buried waste trenches (6 m from the tracer source). The ^3H concentration profiles could be described as sinusoidal functions with local maximum and minimum concentrations within the fracture regime occurring during early December and early April, respectively. Decreasing concentrations of (^3H) in the fracture regime results from dilution arising from a seasonal increase flux of groundwater in response to large rainfall inputs during the winter and early spring. The exact same trends were observed for the Br, He, and Ne tracers (Figs. 7 and 10). An important feature of the contaminant discharge trends show that the sinusoidal functions for the matrix regime progressively shifted to later times in the year with increased distances into the matrix (Fig. 13). The time lags in the concentration profiles of the matrix relative to the fracture were similar to measured first-arrival times of the nonreactive tracers that migrated from the fracture into the surrounding matrix (Table 2). These results showed that indeed the multiple tracer test served as an adequate means of quantifying the rate of contaminant storage and depletion within the shale bedrock matrix.

CONCLUSIONS AND IMPLICATIONS

This paper has presented a field study that was designed to quantify the advective and diffusive mass transfer of solutes in contaminated fractured shale bedrock. Our unique experimental

approach using a long-term natural gradient injection strategy, multiple tracers that had different molecular diffusion coefficients, and the ability to monitor both the matrix and fracture regimes, all served to verify the significance of solute diffusion into the rock matrix. The results of this study showed that secondary contaminant sources form within the bedrock matrix, and that the importance of this source increases with continued contaminant discharge through the bedrock fracture network. This is particularly important for reactive contaminants such as radionuclides, where matrix diffusion can enhance solute retardation by many orders of magnitude. Under certain circumstances the increased retardation may be beneficial; for example, the enhanced retardation of short lived radionuclides such as ^{90}Sr and ^{60}Co (~ 29 and 5 yr, respectively) may allow for their decay in-place, thereby eliminating the need for remediation. In other instances, this secondary contaminant source invokes a severe limitation on the successful removal of contaminants that are too hazardous to reside in the subsurface. Direct experimental measurements of contaminant migration rates into the rock matrix, as presented in this study, have application in risk assessment modeling and in the design of improved remedial strategies targeted at contaminant removal in hard to reach sources within the bedrock matrix. In general, the multiple tracer technique not only improves our conceptual understanding of the time-dependent solute migration in subsurface media, it also provides the necessary experimental constraints that are needed for the accurate numerical quantification of the physical nonequilibrium process. It is a sensitive means by which the significance of diffusion can be quantified for a variety of needs including nutrient use efficiency in crops and trees, resource recovery, waste management, and the remediation of contaminated environments.

ACKNOWLEDGMENTS

This research was supported by the Office of Environmental Management, Oak Ridge National Laboratory and the Environmental Technology Partnership (ETP) program of the Office of Biological and Environmental Research, U.S. Department of Energy. The authors would like to thank Dr. Harry Boston, who was the contract officer for the Environmental Restoration and Waste Management Division, ORNL, and Dr. Paul Bayer, contract officer for DOE's ETP program, for financially supporting this research. Oak Ridge National Laboratory is managed by Lockheed Martin Energy Research Corporation for the U.S. Department of Energy, under contract DE-AC05-96OR22464. Publication No._____, Environmental Sciences Division, ORNL.

REFERENCES

Abelin, H., L. Birgersson, J. Gidlund, L. Moreno, I. Neretnieks, H. Wilden, and T. Agren, 3-D migration experiment - Report 3, part I, Performed experiments, results and evaluation, Tech. Rep. 87-21, Stripa Proj., Stockholm, Nov. 1987.

Abelin, H., L. Birgersson, L. Moreno, H. Wilden, T. Agren, I. Neretnieks, 1991, A large-scale flow and tracer experiment in granite 2. Results and interpretation, Water Resour. Res., 27, 3119-3135, 1991.

Ahn, J., P.L. Chambre, and T.H. Pigford, Radionuclide migration through fractured rock: Effects of multiple fractures and two-member decay chains, Lawrence Berkeley Laboratory, Berkeley, California, LBL-21121, 1985.

Berglund, S., and V. Cvetkovic, Pump-and-treat remediation of heterogeneous aquifers: Effects of rate-limited mass transfer, Ground Water, 33, 675-685, 1995.

Birgersson, L., L. Moreno, I. Neretnieks, H. Widen, and T. Agren, A tracer migration experiment in a small fracture zone in granite, Water Resour. Res., 29, 3867-3878, 1993.

Birgersson, L., and I. Neretnieks, Diffusion in the matrix of granitic rock: Field test in the Stripa Mine, Water Resour. Res., 26, 2833-2842, 1990.

Brogan, S.D., and R.M. Gailey, A method for estimating field-scale mass transfer rate parameters and assessing aquifer cleanup times, Ground Water, 33, 997-1009, 1995.

Cacas, M.C., E. Ledoux, G. De Marsily, B. Tillie, A. Barbreau, E. Durand, B. Feuga, and P. Peaudecerf, Modeling fracture flow with a stochastic discrete fracture network: Calibration and validation. 1. The flow model, Water Resour. Res., 26, 479-489, 1990a.

Cacas, M.C., E. Ledoux, G. De Marsily, A. Barbreau, P. Calmels, B. Gaillard, and R. Margritta, Modeling fracture flow with a stochastic discrete fracture network: Calibration and validation. 2. The transport model, Water Resour. Res., 26, 491-500, 1990b.

Dorsch, J., T.J. Katsube, W.E. Sanford, B.E. Dugan, and L.M. Tourkow, Effective porosity and pore-throat size of Conasauga group mudrock: Application, test and evaluation of petrophysical techniques. Oak Ridge National Laboratory, Oak Ridge, Tennessee, ORNL/GWPO-02 1, 1996.

Dreier, R.B., D.K. Solomon, and C.M. Beaudoin, Fracture characterization in the unsaturated zone of a shallow land burial facility, in Flow and Transport Through Unsaturated Rock, edited by D.D. Evans and T. J. Nicholson, Geophysical Monograph 42, 51-59, 1987.

Drost, W., D. Klotz, A. Koch, H. Moser, F. Neumaier, and W. Rauert, Point dilution methods of investigating groundwater flow by means of radioisotopes, Water Resour. Res., 4, 125-146, 1968.

Environmental Protection Agency, Prescribed procedures for measurement of radioactivity in drinking water, Environmental Monitoring and Support Laboratory, Cincinnati, OH, EPA-600/4-80-032, 1980.

Freyberg, D.L., A natural gradient experiment on solute transport in a sand aquifer. 2. Spatial moments and the advection and dispersion of nonreactive tracers, Water Resour. Res., 22, 2031-2046, 1986.

Frohne, K.-H., and J.C. Mercer, Fractured shale gas reservoir performance study - An offset well interference field test, J. Petroleum Technol., 36, 291-300, 1984.

Garnier, J.M., N. Crampon, C. Preaux, G. Porel, and M. Vreulx, Tracage par ^{13}C, ^{2}H, and I et uranine dans la nappe de la craie senonienne en ecoulement radial convergent (Bethune, France), J. Hydrol. Amsterdam, 78, 379-392, 1985.

Gwo, J.P, P.M. Jardine, G.V. Wilson, and G.T. Yeh, A multiple-pore-region concept to modeling mass transfer in subsurface media, J. Hydrol., 164, 217-237, 1995.

Gwo, J.P., P.M. Jardine, G.V. Wilson, and G.T. Yeh, Using a multiregion model to study the effects of advective and diffusive mass transfer on local physical nonequilibrium and solute mobility in a structured soil, Water Resour. Res., 32, 561-570, 1996.

Gwo, J.P., R. O'Brien, and P.M. Jardine, Mass transfer in structured porous media: embedding mesoscale structure and microscale hydrodynamics in a two-region model, J. Hydrol., 208, 204-222, 1998.

Haines, B.L., J.B. Waide, and R.L. Todd, Soil solution nutrient concentrations sampled with tension and zero-tension lysimeters: report of discrepancies, Soil Sci. Soc. Am. J., 46, 658-661, 1982.

Halevy, E., H. Moser, O. Zellhofer, and A. Zuber, Borehole dilution techniques: A critical review, Isotopes in Hydrology, IAEA, Vienna, 53 1-564, 1967.

Harvey, R.W., N.E. Kinner, D. MacDonald, D.W. Metge, and A. Bunn. Transport behavior of groundwater protozoa and protozoan-sized microspheres in sandy aquifer sediments. Applied and Environmental Microbiology, Jan, pp. 209-2 17, 1995.

Harvey, R.W., L.H. George, R.L. Smith, and D.L. LeBlanc. Transport of microspheres and indigenous bacteria through a sandy aquifer: Results of natural- and forced-gradient tracer experiments. Sci. Technol., 23, 51-56, 1989.

Harvey, R. W., N.E. Kinner, D. MacDonald, D. W. Metge, and A. Bunn. Role of physical heterogeneity in the interpretation of small-scale laboratory and field observations of bacteria, microbial-sized microsphere, and bromide transport through aquifer sediments. Water Resourc. Res., 29, 2713-2721, 1993.

Hicks, D.S., D.K. Solomon, and N.D. Farrow, Investigation of groundwater flow zones and contaminant transport in solid waste storage area 5 at Oak Ridge National Laboratory, Oak Ridge, Tennessee, U.S. Dep. of Energy, ORNL/ER-Report 154, 1992.

Holtta, P., M. Hakanen, A. Hautojarvi, J. Timonen, K. Vaatainen, The effect of matrix diffusion on radionuclide migration in rock column experiments, J. Contam. Hydrol., 2 1, 165-173, 1996.

Jardine, P.M., G.V. Wilson, and R. J. Luxmoore, Modeling the transport of inorganic ions through undisturbed soil columns from two contrasting watersheds, Soil Sci. Soc. Am. J., 52, 1252-1259, 1988.

Jardine, P.M., G.V. Wilson, R.J. Luxmoore, and J.F. McCarthy. Transport of inorganic and natural organic tracers through an isolated pedon in a forested watershed. Soil Sci. Soc. Am. J., 53, 317-323, 1989.

Jardine, P.M., G.V. Wilson, and R.J. Luxmoore, Unsaturated solute transport through a forest soil during rain storm events, Geoderma, 46, 103-1 18, 1990a.

Jardine, P.M., G.K. Jacobs, and G.V. Wilson, Unsaturated transport processes in undisturbed heterogeneous porous media: I. Inorganic contaminants, Soil Sci. Soc. Am. J., 57, 945-953, 1993a.

Jardine, P.M., G.K. Jacobs, and J.D. O'Dell. Unsaturated transport processes in undisturbed heterogeneous porous media: II. Co-contaminants. Soil Sci. Soc. Am. J., 57, 954-962, 1993b.

Jardine, P.M., R. O'Brien, G.V. Wilson, and J.P. Gwo, Experimental techniques for confirming and quantifying physical nonequilibrium processes in soils, in Physical nonequilibrium in soils: Modeling and application, edited by Selim, H.M., and L. Ma, Ann Arbor Press Inc., Chelsea, Michigan, 243-266, 1998.

Jaynes, D.B., and R. Horton. Field parameterization of the mobile/immobile domain model, in Physical nonequilibrium in soils: Modeling and application, edited by Selim, H.M., and L. Ma, Ann Arbor Press Inc., Chelsea, Michigan, 297-309, 1998.

Khire, J.M., and M.I. Khan, Microbially enhanced oil recovery (MEOR). Part 1. Importance and mechanism of MEOR, Enzyme Microb. Technol., 16, 170-172, 1994a.

Khire, J.M., and M.I. Khan, Microbially enhanced oil recovery (MEOR). Part 2. Microbes and the subsurface environment for MEOR, Enzyme Microb. Technol., 16, 258-259, 1994b.

Lawes, J.B., J.H. Gilbert, and R. Warington, On the amount and composition of the rain and drainage waters collected at Rothamsted. III. The drainage water from land cropped and manured, J. R. Agric. Soc. Engl., 18, 1- 17, 1882.

Lee, R.R., R.H. Ketelle, J.M. Bownds, and T.A. Rizk. Aquifer analysis and modeling in a fractured, heterogeneous medium. Ground Water, 30, 589-597, 1992.

Maloszewski, P., and A. Zuber. Mathematical modeling of tracer behavior in short-term experiments in fissured rocks. Water Resourc. Res., 26, 15 17-1528, 1990.

Maloszewski, P., and A. Zuber. Tracer experiments in fractured rocks: Matrix diffusion and the validity of models. Water Resourc. Res., 29, 2723-2735, 1993.

McKay, L.D., R.W. Gillham, and J.A. Cherry, Field experiments in a fractured clay till. 2. Solute and colloid transport, Water Resourc. Res., 29, 3879-3890, 1993a.

McKay, L.D., J.A. Cherry, R.C. Bales, M.T. Yahya, and C.P. Gerba. A field example of bacteriophage as tracers of fracture flow. Environ. Sci. Technol., 27, 1075-1079, 1993b.

McKay, L.D., W.E. Sanford, J.M. Strong-Gunderson, and V. De Enriquez. Microbial tracer experiments in a fractured weathered shale near Oak Ridge, Tennessee. International Assoc. Hydrogeologists Congress, Edmonton, Alberta, Canada, June 5-10, 1995.

Moline, G.R., M.E. Schreiber, and J.M. Bahr, Representative groundwater monitoring in fractured porous systems, J. Environ. Engineering, 124(6), 530-538, 1998.

Neretnieks, I., Diffusion in the rock matrix: An important factor in radionuclide retardation?, J. Geophys. Res., 85, 4379-4397, 1980.

Neretnieks, I., Solute transport in fractured rock - Applications to radionuclide waste repositories, in Flow and Contaminant Transport in Fractured Rock, edited by J. Baer, C.-F. Tsang, and G. de Marsily, pp. 39- 127, Academic Press, New York, New York, 1993.

Novakowski, K.S., and P.A. Lapcevic, Field measurement of radial solute transport in fractured rock, Water Resour. Res., 30, 37-44, 1994.

Novakowski, K. S., P. A. Lapcevic, J. Voralek, and G. Bickerton, Preliminary interpretation of tracer experiments conducted in a discrete rock fracture under conditions of natural flow, Geophysical Research Letters, 22, 14 17- 1420, 1995.

Raven, K.G., K. S. Novakowski, and P.A. Lapcevic. Interpretation of field tracer tests of a single fracture using a transient solute storage model. Water Resourc. Res., 24, 2019-2032, 1988.

Reedy, O.C., P.M. Jardine, G.V. Wilson, and H.M. Selim, Quantifying the diffusive mass transfer of nonreactive solutes in columns of fractured saprolite using flow interruption, Soil Sci. Soc. Am. J., 60, 1376-1384, 1996.

Ronen, D., Y. Yechieli, and A. Kribus, Buoyancy-induced flow of a tracer in vertical conduits, Water Resour. Res., 3 1, 1167-1 173, 1995.

Sanford, W.E., and G.K. Moore, Measurement of specific discharge with point-dilution tests in the fractured rocks of eastern Tennessee, Proceedings of Extended Abstracts, American Water Resources Association, Annual Spring Symposium, Nashville, Tennessee, pp. 449-453, 1994.

Sanford, W.E., R.G. Shropshire, and D.K. Solomon. Dissolved gas tracers in groundwater: Simplified injection, sampling, and analysis. Water Resorc. Res., 32, 1635-1642, 1996.

Sanford, W.E., and D.K. Solomon. The influence of matrix diffusion on tracer transport, EOS Transactions, American Geophysical Union, Spring Meeting, v 77, no. 17, p. S108, 1996.

Sanford, W.E., and D.K. Solomon, Using dissolved gases for site characterization and containment assessment, J. Environ. Engineering, 124, 572-574, 1998.

Schettler, P.D., and C.R. Parmely, Physicochemical properties of methane storage and transport in Devonian shale. Final report April 1985 - April 1991. Juniata Coll., Huntingdon, PA, PB-94-120359/XAB, 51 p., 1993.

Schumacher, W. Die Physik des Bodens, Berlin, 1864.

Selim, H.M., and L. Ma, Physical nonequilibrium in soils: Modeling and application, Ann Arbor Press Inc., Chelsea, Michigan, 1998.

Seyfried, M. S., and P. S.C. Rao, Solute transport in undisturbed columns of an aggregated tropical soil: Preferential flow effects, Soil Sci. Soc. Am. J., 5 1, 1434-1444, 1987.

Shaffer, K.A., D.D. Fritton, and D.E. Baker, Drainage water sampling in a wet, dual-pore soil system, J. Environ. Qual., 8, 24 1-246, 1979.

Shevenell, G.K., G.K. Moore, and R.B. Dreier, Contaminant spread and flushing in fractured rocks near Oak Ridge, Tennessee, Ground Water Monitoring and Remediation, Spring, 120-129, 1994.

Shuford, J.W., D.D. Fritton, and D.E. Baker, Nitrate-nitrogen and chloride movement through undisturbed field soil, J. Environ. Qual., 6, 255-259, 1977.

Sledz, J.J., and D.D. Huff, Computer model for determining fracture porosity and permeability in the Conasauga Group. Oak Ridge National Laboratory, Oak Ridge, Tennessee, ORNL/TM-7695, 1981.

Solomon, D.K., G.K. Moore, L.E. Toran, R.B. Drier, and W.M. McMaster, A hydrologic framework for the Oak Ridge Reservation, Oak Ridge National Laboratory, Oak Ridge, Tennessee, ORNL/TM- 12026, 1992.

Sudicky, E.A., and E.O. Frind, Contaminant transport in fractured porous media: Analytical solutions for a system of parallel fractures. Water Resour. Res., 18, 1634-1642, 1982.

Toran, L., A. Sjoreen, and M. Morris, Sensitivity analysis of solute transport in fractured porous media, Geophysical Research Letters, 22, 143 3 - 143 6, 1995.

Vandergraaf, T.T., D. J. Drew, and S. Masuda, Radionuclide migration experiments in a natural fracture in a quarried block of granite, J. Contam. Hydrol., 2 1, 153-164, 1996.

Walter, G.R., Theoretical and experimental determination of matrix diffusion and related solute transport properties of fractured tuffs from the Nevada Test Site, Los Alamos National Laboratory, Los Alamos, New Mexico, LA-9471-MS, 1982.

Wickliff, D.S., D.K. Solomon, and N.D. Farrow, Preliminary investigation of processes that affect source term identification, Oak Ridge National Laboratory, Oak Ridge, Tennessee, U.S. Dep. of Energy, ORNL/ER-Report 59, 1991.

Wilson, G.V., P.M. Jardine, R. J. Luxmoore, L. W. Zelazny, D.A. Lietzke, and D.E. Todd. Hydrogeochemical processes controlling subsurface transport from an upper subcatchment of Walker Branch watershed during storm events. 1. Hydrologic transport processes. J. Hydrol., 123, 297-316, 1991a.

Wilson, G.V., P.M. Jardine, R. J. Luxmoore, L. W. Zelazny, D.E. Todd, and D.A. Lietzke. Hydrogeochemical processes controlling subsurface transport from an upper subcatchment of Walker Branch watershed during storm events. 2. Solute transport processes. J. Hydrol., 123, 317-336, 1991b.

Wilson, G.V., P.M. Jardine, and J.P. Gwo. Modeling the hydraulic properties of a multiregion soil. Soil Sci. Soc. Am. J., 56, 1731-1737, 1992.

Wilson, G.V., P.M. Jardine, J.D. O'Dell, and M. Collineau, Field-scale transport from a buried line source in variable saturated soil, J. Hydrol., 145, 83-109, 1993.

Table 1: Well locations in the fracture or matrix regime as determined by Br^- first arrival times and peak breakthrough concentrations.

Well ID	Horizontal distance from source (m)	Time of Br^- first arrival (d)	Approx. peak concentration Br^- as c/c_o [+]	Presumed fracture (F) & matrix (M) regime
1	-1.83	ND	0	-
2	0	ND	0	
3	0	ND	0	-
4	3.40	ND	0	-
5	2.80	ND	0	-
6	5.40	101	0.006	M
7	6.00	3	0.10	M
8	6.00	50	0.05	M
9	6.00	0.9	0.30	F
10	6.40	< 0.9	0.35	F
11	5.40	ND	0	–
12	6.00	ND	0	–
13	6.40	ND	0	–
4165-A	6.00	*	–	
4165-B	6.00	3	0.07	F
4165-C	6.00	1	0.08	F
4165-D	6.00	< 0.9	0.35	F
14	9.00	84	0.01	M
15	9.20	81	0.009	M
16	9.20	3	0.20	F
17a	13.20	25	0.16	M
17b	16.50	100	0.015	M
2046-A	16.80	15	0.13	F
2046-B	16.80	5	0.14	F
2046-C	16.80	3	0.15	F
2046-D	16.80	3	0.19	F
2046-E	16.80	6	0.04	M
18a	23.70	21	0.06	M
18b	26.80	ND	0	M
19a	30.60	143	0.065	M
19b	30.80	143	0.065	M
19c	31.00	105	0.06	M
20	35.20	110	0.023	M

[+] c_o = injection concentration of 1159 μg Br^- mL^{-1} with the peak concentration estimated from visual smoothing of the Br^- breakthrough curves; ND = None detected; * = faulty sampler

Table 2: Comparison of Br^- first arrive times with ^3H concentration lag times, for various distances into the matrix and 6 m from the source.

Distance into matrix from fracture regime (m)	Br^- first arrival (d)	^3H lag time (max/min) (d)
0.02	**3**	**7**
0.79	**50**	**45**
1.38	**101**	**75**

Regression of Br^- arrival times vs. ^3H lag times: r^2=0.996, slope=0.69, intercept=6.8

LIST OF FIGURES

Figure 1

Schematic diagram of Waste Area Grouping 5 (WAG 5) showing the location of buried waste trenches and the location of the experimental field facility with a few examples of groundwater monitoring wells (4014, 4165, 2065) that have been strategically placed strike parallel.

Figure 2

Cross-section of the experimental field facility showing specific discharge measurements as a function of depth in wells 4165 and 2046, and at a single depth for well 4014. Black bars along the specific discharge y-axes indicate the position of multilevel groundwater samplers.

Figure 3

Map view of the groundwater monitoring well locations and surface topography of the field facility. Wells 4014, 4165, and 2065 were wet rotary cored to 9 m, with well 4014 serving as the tracer injection well. Wells 1 through 20 were drive-point wells that were placed at a variety of depths using a track-mounted pneumatic hammer. The wells form a strike parallel transect from the waste trenches to a seep that drains into a cross-cutting tributary (modified from Sanford et al., 1996).

Figure 4

Cross-section of the experimental field facility showing the location and sampling depth of all groundwater monitoring wells, with well 4014 serving as the tracer injection well (see figure 2). The approximate locations of the fracture and matrix regimes are also illustrated.

Figure 5

Daily rainfall (a) and examples of bromide breakthrough at 6, 17, and 31 m from the source (b). Breakthrough curves represent Br^- transport in wells 10, 2046-D, and 19c, respectively, that are located within, or close to, the faster flowing fracture regime of the bedrock formation. Relative time on the x-axis is based on t=0 at October 18, 1994.

Figure 6

Cross-section of Br^- concentration contours at the experimental field facility, 77, 185, and 233 days following the initiation of tracer injection. Recall tracer was continuously injected for 180 d within the fracture regime of well 4014. Bromide concentrations are shown as $\mu g\ mL^{-1}$ with each contour representing an increment of 25 mg Br L^{-1}. Symbol + represents the bottom position of the drive-point wells detailed in figure 4.

Figure

Daily rainfall (a) and bromide breakthrough (b,c) at 6 m from the source within the fracture (wells 9 and 10) and matrix regimes (wells 6, 7, 8). Figure c shows an expanded y-axis of b which details Br^- breakthrough into the matrix regime 0.8 m and 1.4 m from the fracture regime.

Figure

Daily rainfall (a) and bromide breakthrough (b,c) at 9 m from the source within the fracture regime (well 16) and matrix regime (wells 14, 15). Note y-axis scale change for b and c.

Figure 9

Observed and model simulated breakthrough curves for Br within the matrix and fracture regimes (a and b, respectively) at various distances from the source, where θ=0.20 is the porosity, 2b=8.4 E-5 m is the fracture aperture, 2B=2.0 m is the fracture spacing, v=100 m d^{-1} is the mean pore water velocity within the fracture regime, α=0.1 m is the dispersivity, τ=0.6 is the tortuosity, and z is the distance into the matrix

Figure 10

Observed breakthrough of He, Ne, and Br within the fracture regime, 6 m (well 10) and 9 m (well 16) from the source (a and b, respectively).

Figure 11

Observed breakthrough of He, Ne, and Br within the matrix regime, at 6 m (well 8), 13 m (well 17a), and 23 m (well 18a) from the source (a, b, c, respectively).

Figure 12

Observed and model simulated breakthrough curves for He, Ne, and Br within the matrix regime, 6 m (a), 13 m (b), and 23 m (c) from the source, where θ=0.20 is the porosity, 2b=8.4 E-5 m is the fracture aperture, 2B=2.0 m is the fracture spacing, v=100 m d^{-1} is the mean pore water velocity within the fracture regime, α=0.1 m is the dispersivity, τ=0.6 is the tortuosity, and z is the distance into the matrix.

Figure 13

Observed ^3H concentration profiles as a function of time within the fracture (well 10) and matrix (wells 6, 7, 8) regimes, 7.6 m downgradient from the buried waste trenches (6 m from injection well 4014).

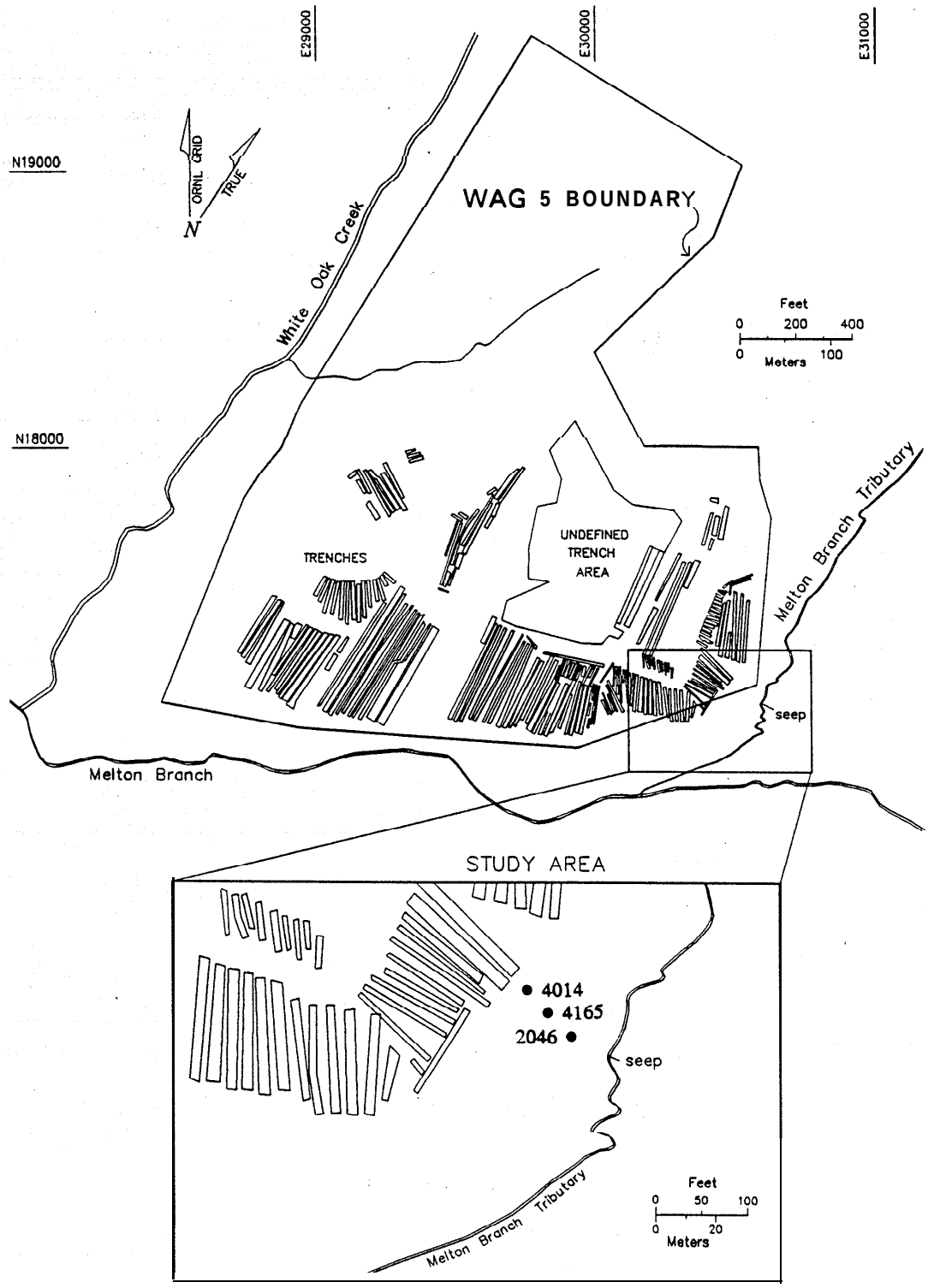
E29000
E30000
E31000
N19000
N18000
ORNL GRID
TRUE
N
WAG 5 BOUNDARY
White Oak Creek
Feet
0 200 400
0 Meters 100
TRENCHES
UNDEFINED TRENCH AREA
Melton Branch Tributary
seep
Melton Branch
STUDY AREA
4014
4165
2046
seep
Melton Branch Tributary
Feet
0 50 100
0 20 Meters

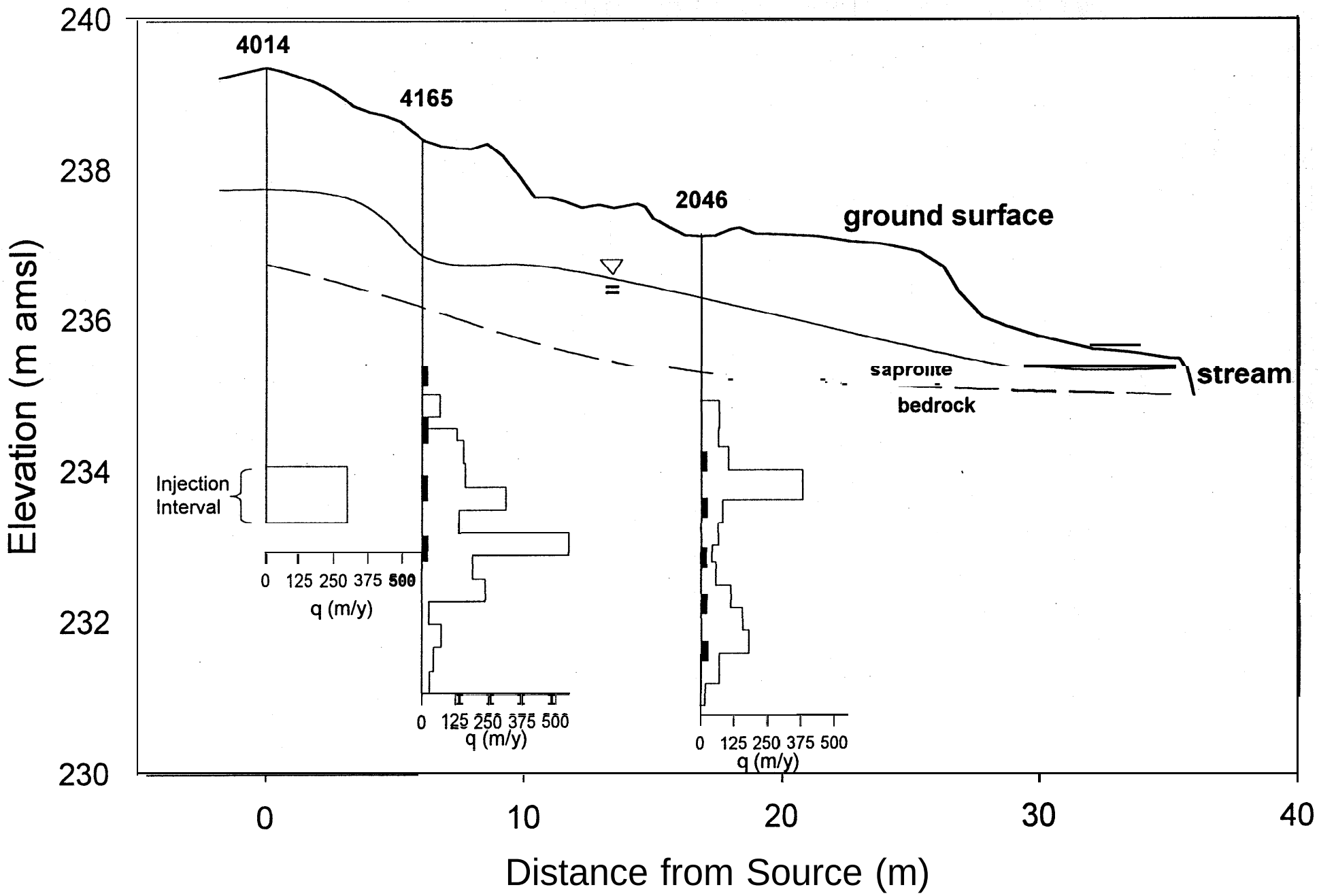
240
238
236
234
232
230
Elevation (m amsl)
4014
4165
2046
ground surface
stream
saprolite
bedrock
Injection
Interval
0 125 250 375 500
q (m/y)
0 125 250 375 500
q (m/y)
0 125 250 375 500
q (m/y)
0
10
20
30
40
Distance from Source (m)

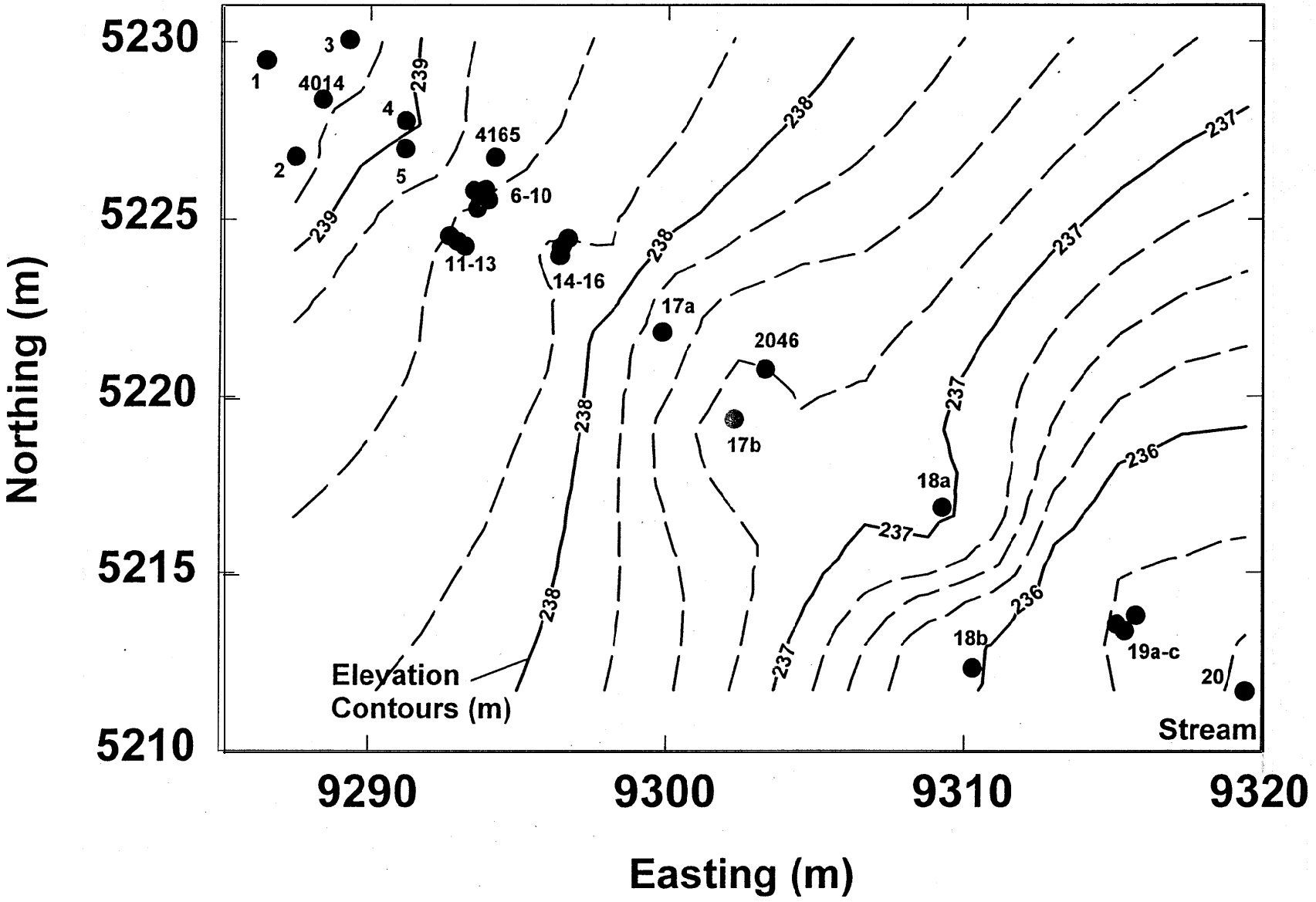
5230
5225
5220
5215
5210
Northing (m)
9290
9300
9310
9320
Easting (m)
1
2
3
4014
4
5
4165
6-10
11-13
14-16
17a
2046
17b
18a
18b
19a-c
20
239
238
237
236
Elevation
Contours (m)
Stream

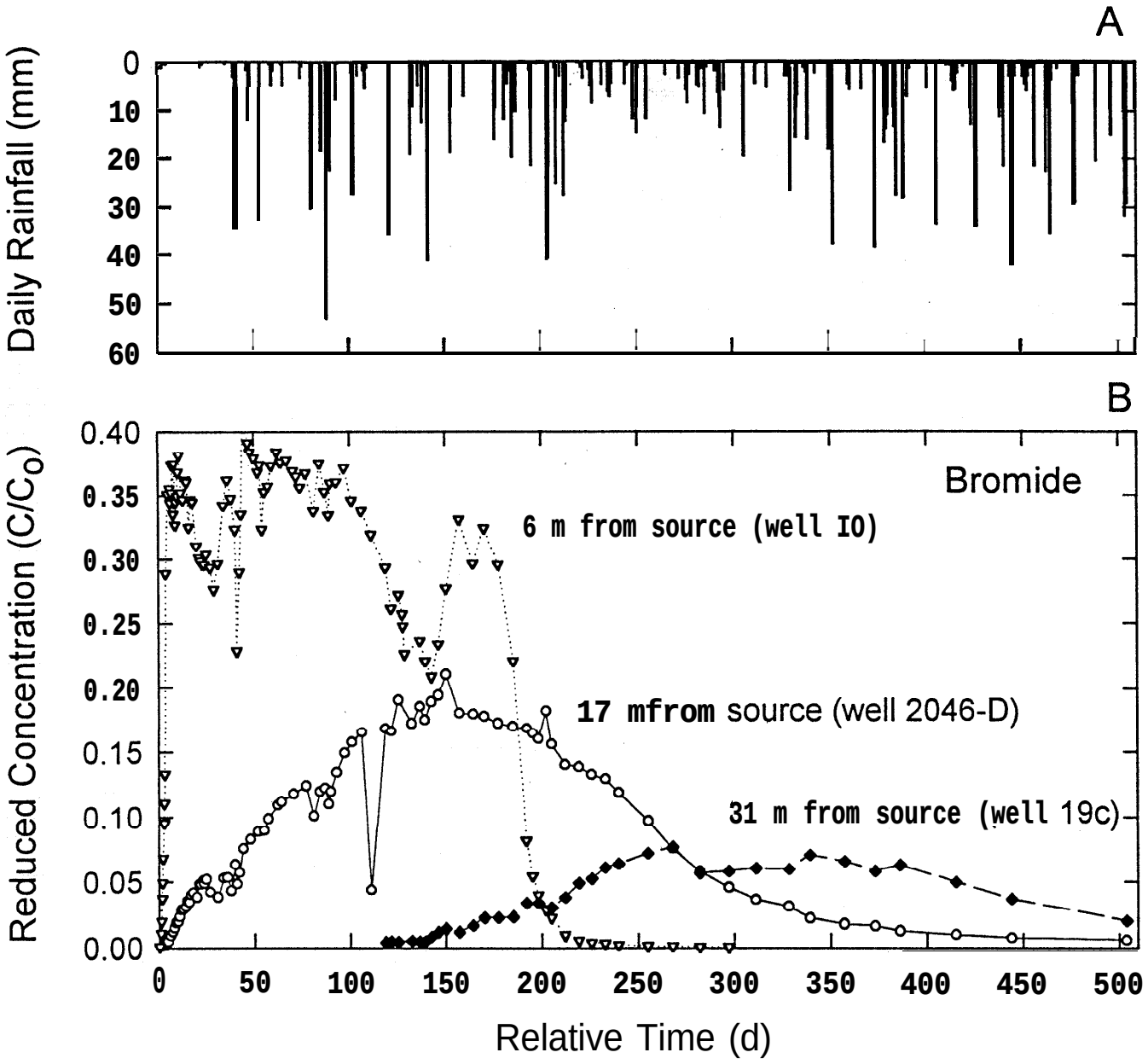
A
Daily Rainfall (mm)
0
10
20
30
40
50
60
B
Reduced Concentration (C/C0)
0.40
0.35
0.30
0.25
0.20
0.15
0.10
0.05
0.00
Bromide
6 m from source (well IO)
17 mfrom source (well 2046-D)
31 m from source (well 19c)
0
50
100
150
200
250
300
350
400
450
500
Relative Time (d)

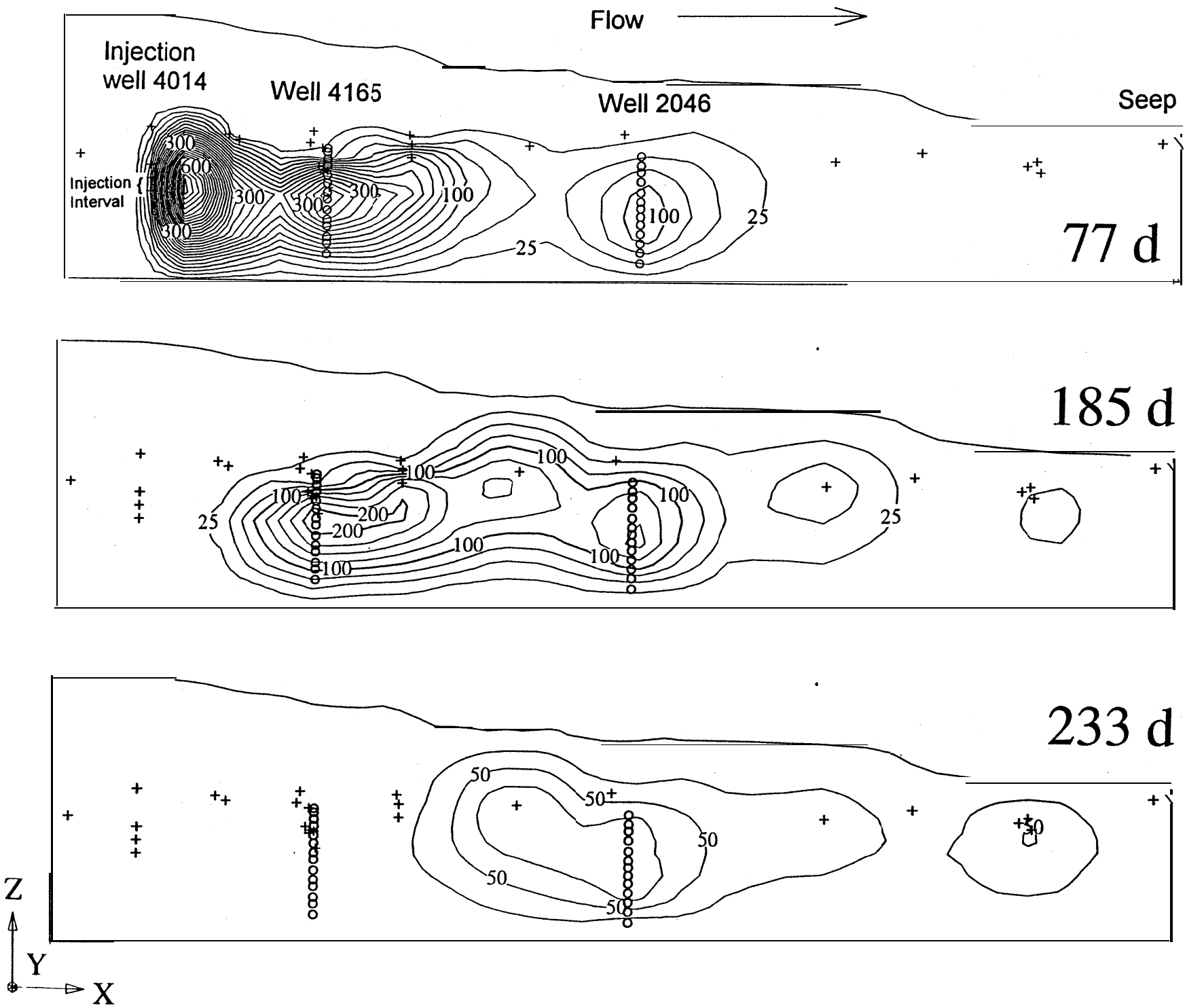
Flow
Injection well 4014
Well 4165
Well 2046
Seep
Injection Interval
300
600
300
300
300
300
100
100
25
25
77 d
185 d
100
100
100
100
100
100
100
200
200
25
25
233 d
50
50
50
50
50
50
50
Z
Y
X

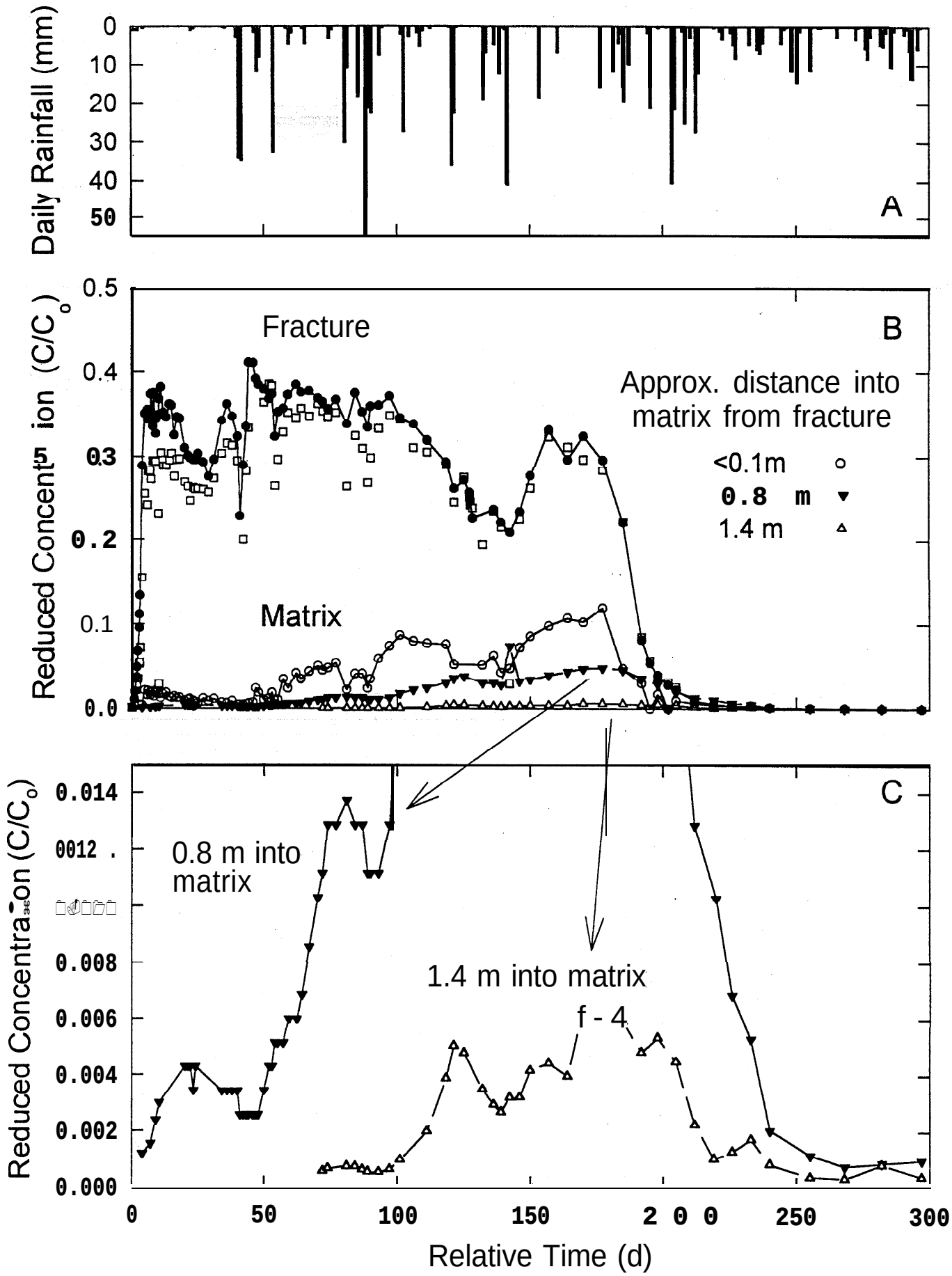
Daily Rainfall (mm)
0
10
20
30
40
50
A
Reduced Concentration (C/C$_o$)
0.5
0.4
0.3
0.2
0.1
0.0
Fracture
B
Approx. distance into matrix from fracture
<0.1m
0.8 m
1.4 m
Matrix
Reduced Concentration (C/C$_o$)
0.014
0.012
0.008
0.006
0.004
0.002
0.000
C
0.8 m into matrix
1.4 m into matrix
f - 4
0
50
100
150
200
250
300
Relative Time (d)

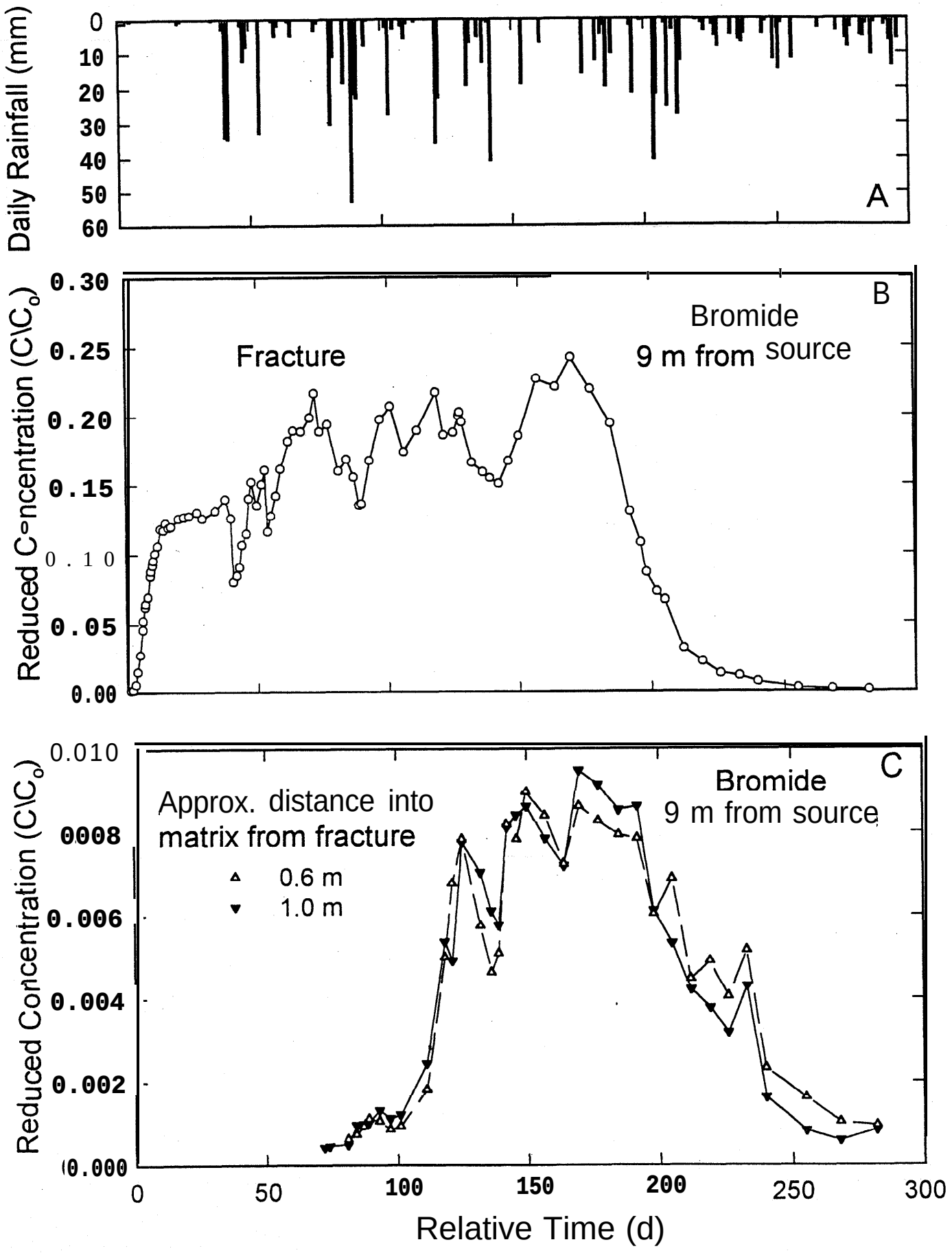
Daily Rainfall (mm)
0
10
20
30
40
50
60
A
Reduced Concentration (C\C$_o$)
0.30
0.25
0.20
0.15
0.10
0.05
0.00
B
Fracture
Bromide
9 m from source
Reduced Concentration (C\C$_o$)
0.010
0008
0.006
0.004
0.002
0.000
C
Approx. distance into
matrix from fracture
0.6 m
1.0 m
Bromide
9 m from source
0
50
100
150
200
250
300
Relative Time (d)

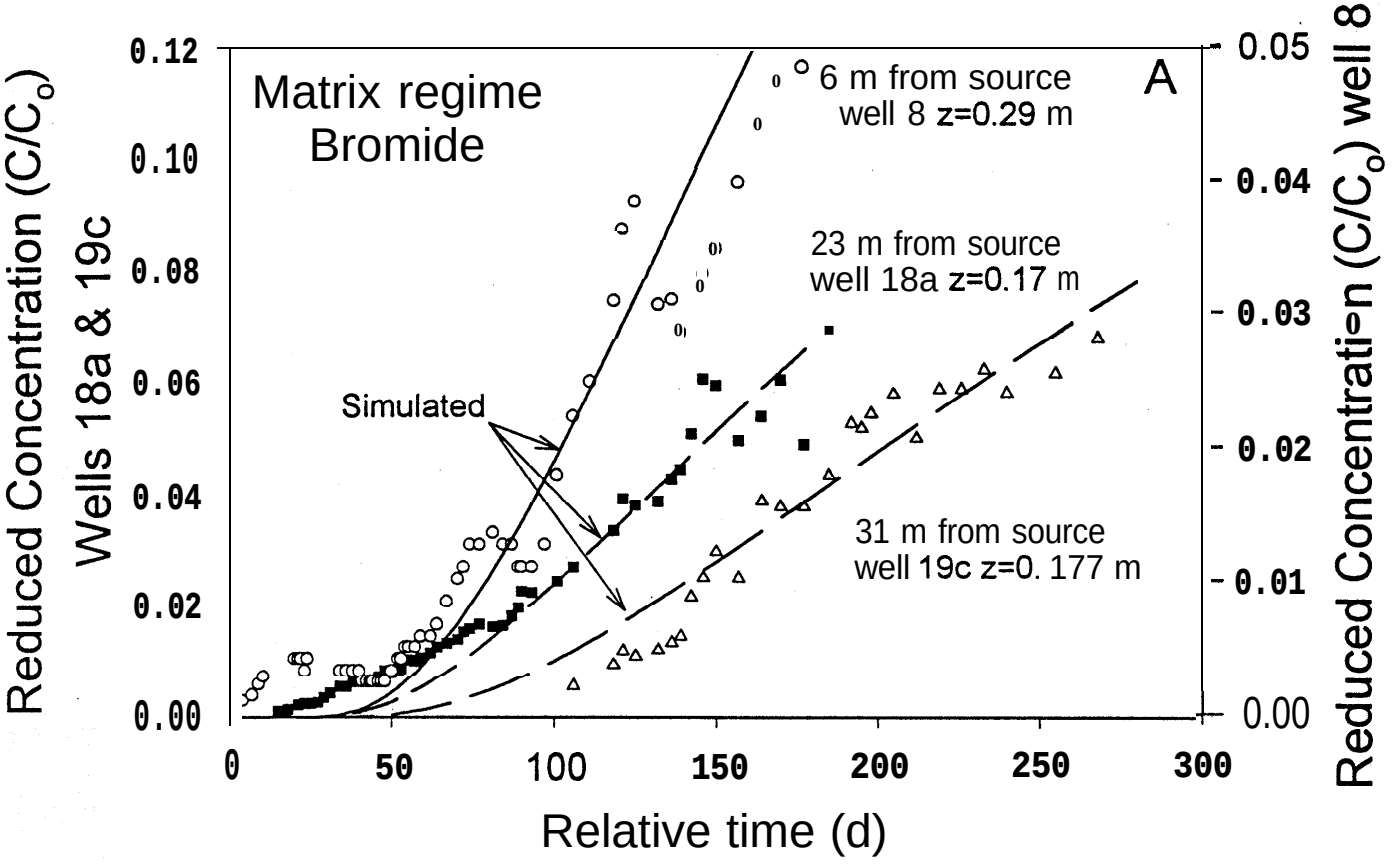
Matrix regime
Bromide
A
6 m from source
well 8 z=0.29 m
23 m from source
well 18a z=0.17 m
31 m from source
well 19c z=0. 177 m
Simulated
Reduced Concentration (C/C$_o$)
Wells 18a & 19c
Reduced Concentrati=n (C/C$_o$) well 8
Relative time (d)
0.12
0.10
0.08
0.06
0.04
0.02
0.00
0.05
0.04
0.03
0.02
0.01
0.00
0
50
100
150
200
250
300

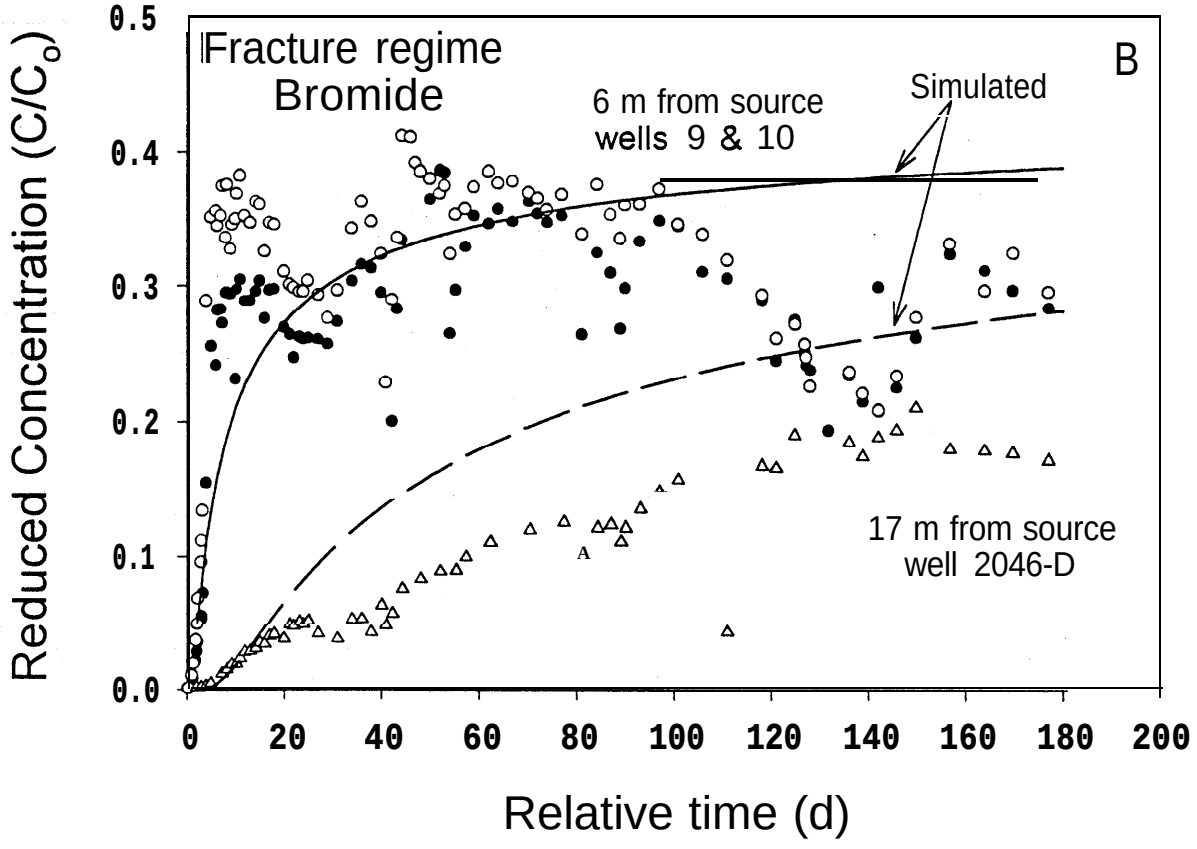
Fracture regime
Bromide
B
6 m from source
wells 9 & 10
Simulated
17 m from source
well 2046-D
Reduced Concentration (C/C$_o$)
Relative time (d)
0.5
0.4
0.3
0.2
0.1
0.0
0
20
40
60
80
100
120
140
160
180
200

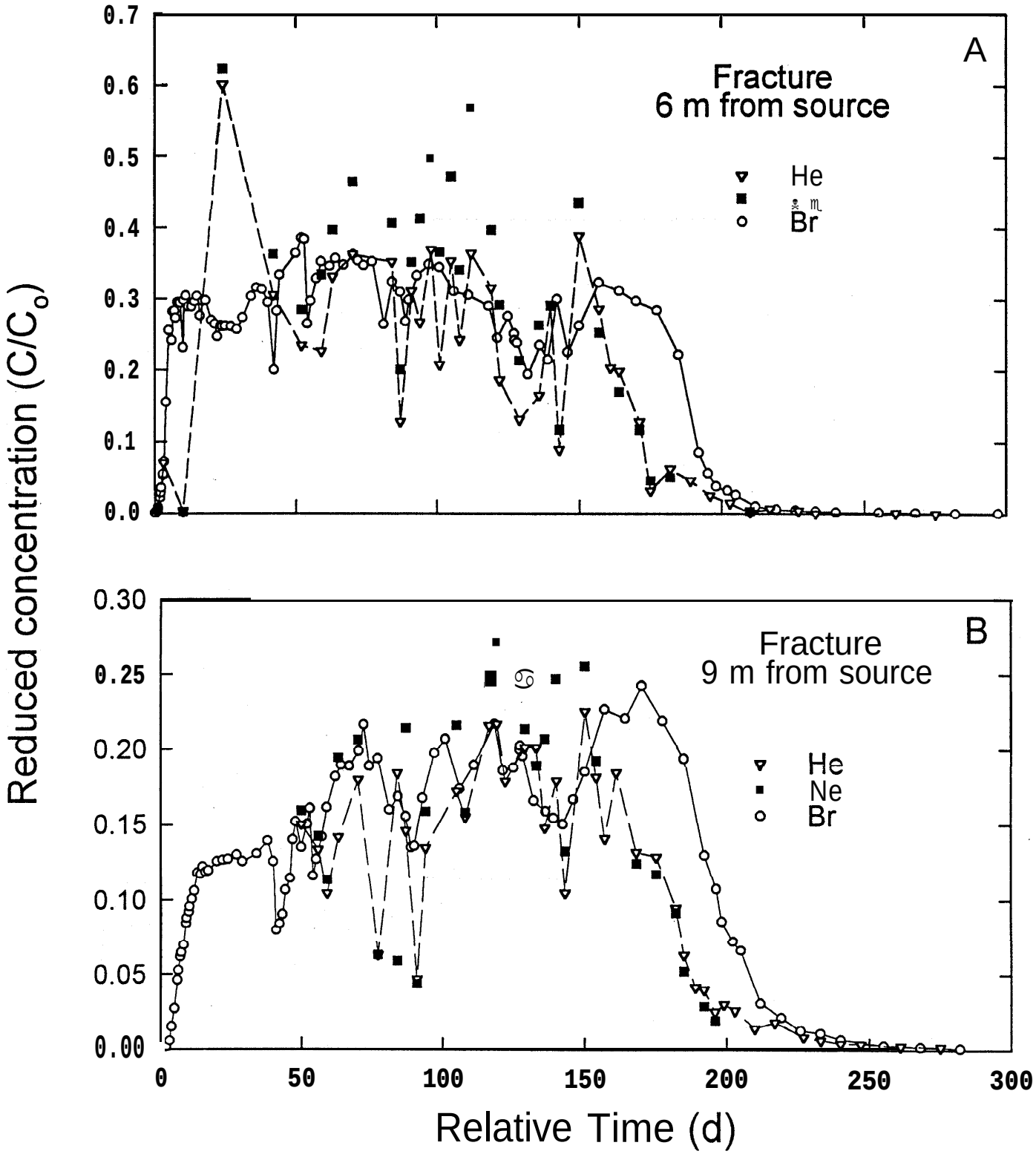
A
Fracture
6 m from source
He
Br
B
Fracture
9 m from source
He
Ne
Br
Reduced concentration (C/C$_o$)
Relative Time (d)
0.7
0.6
0.5
0.4
0.3
0.2
0.1
0.0
0.30
0.25
0.20
0.15
0.10
0.05
0.00
0
50
100
150
200
250
300

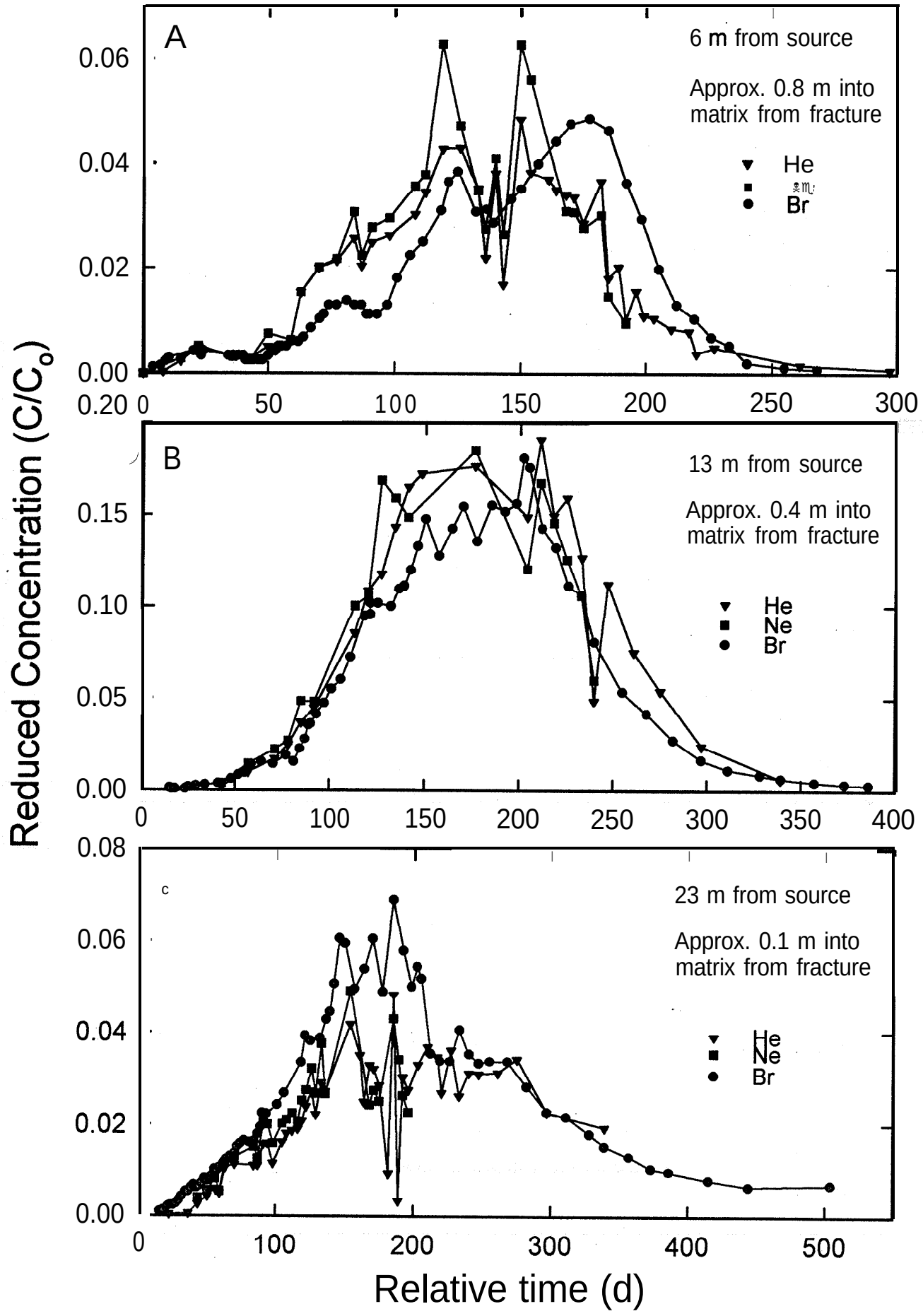
A
6 m from source
Approx. 0.8 m into matrix from fracture
He
Br
B
13 m from source
Approx. 0.4 m into matrix from fracture
He
Ne
Br
C
23 m from source
Approx. 0.1 m into matrix from fracture
He
Ne
Br
Reduced Concentration (C/C$_o$)
Relative time (d)
0.06
0.04
0.02
0.00
0.20
0.15
0.10
0.05
0.08
0
50
100
150
200
250
300
350
400
500

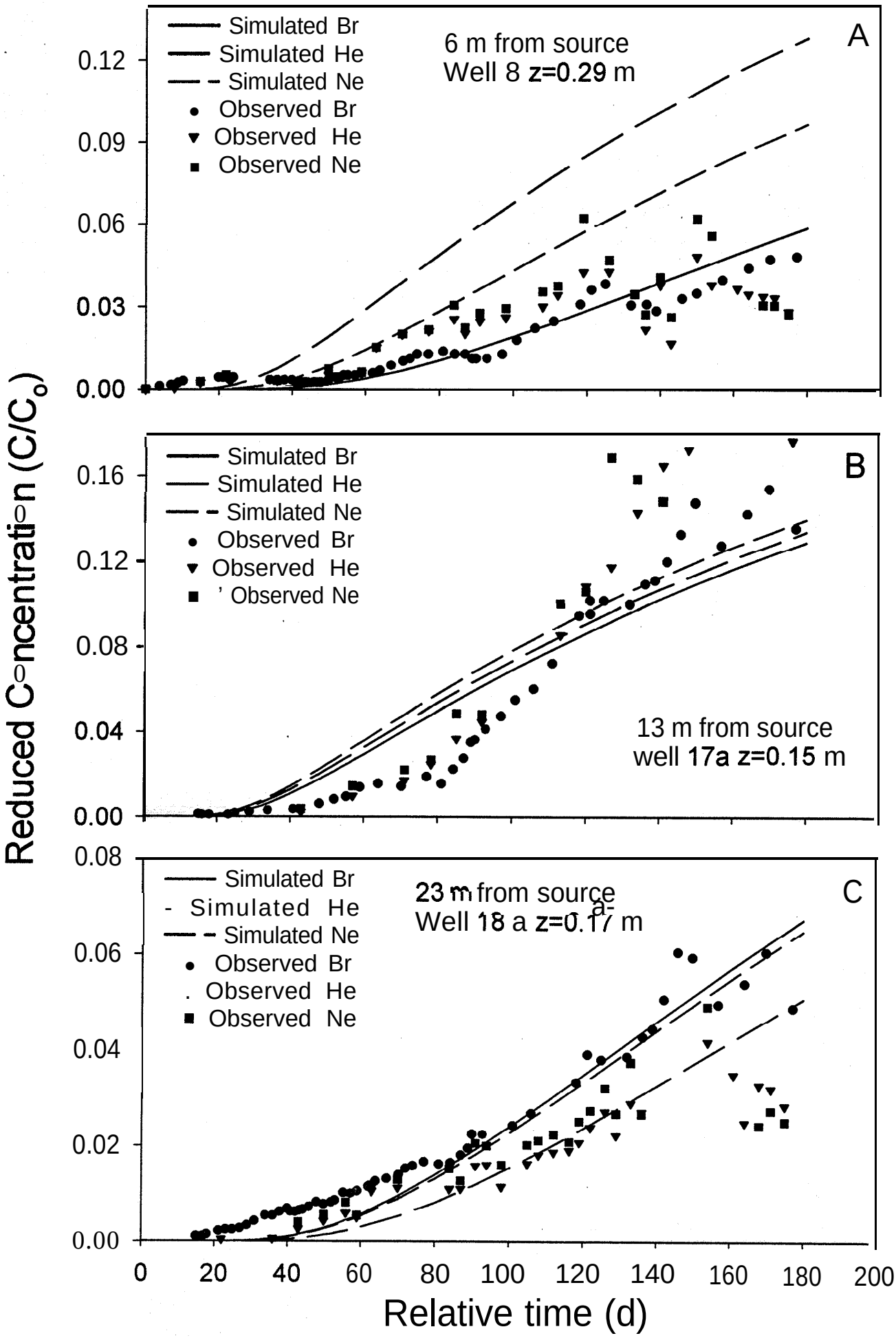
Simulated Br
Simulated He
Simulated Ne
Observed Br
Observed He
Observed Ne
6 m from source
Well 8 z=0.29 m
A
0.12
0.09
0.06
0.03
0.00
Simulated Br
Simulated He
Simulated Ne
Observed Br
Observed He
Observed Ne
B
0.16
0.12
0.08
0.04
0.00
13 m from source
well 17a z=0.15 m
Simulated Br
Simulated He
Simulated Ne
Observed Br
Observed He
Observed Ne
23 m from source
Well 18 a z=0.17 m
C
0.08
0.06
0.04
0.02
0.00
0
20
40
60
80
100
120
140
160
180
200
Relative time (d)
Reduced Concentration (C/C0)

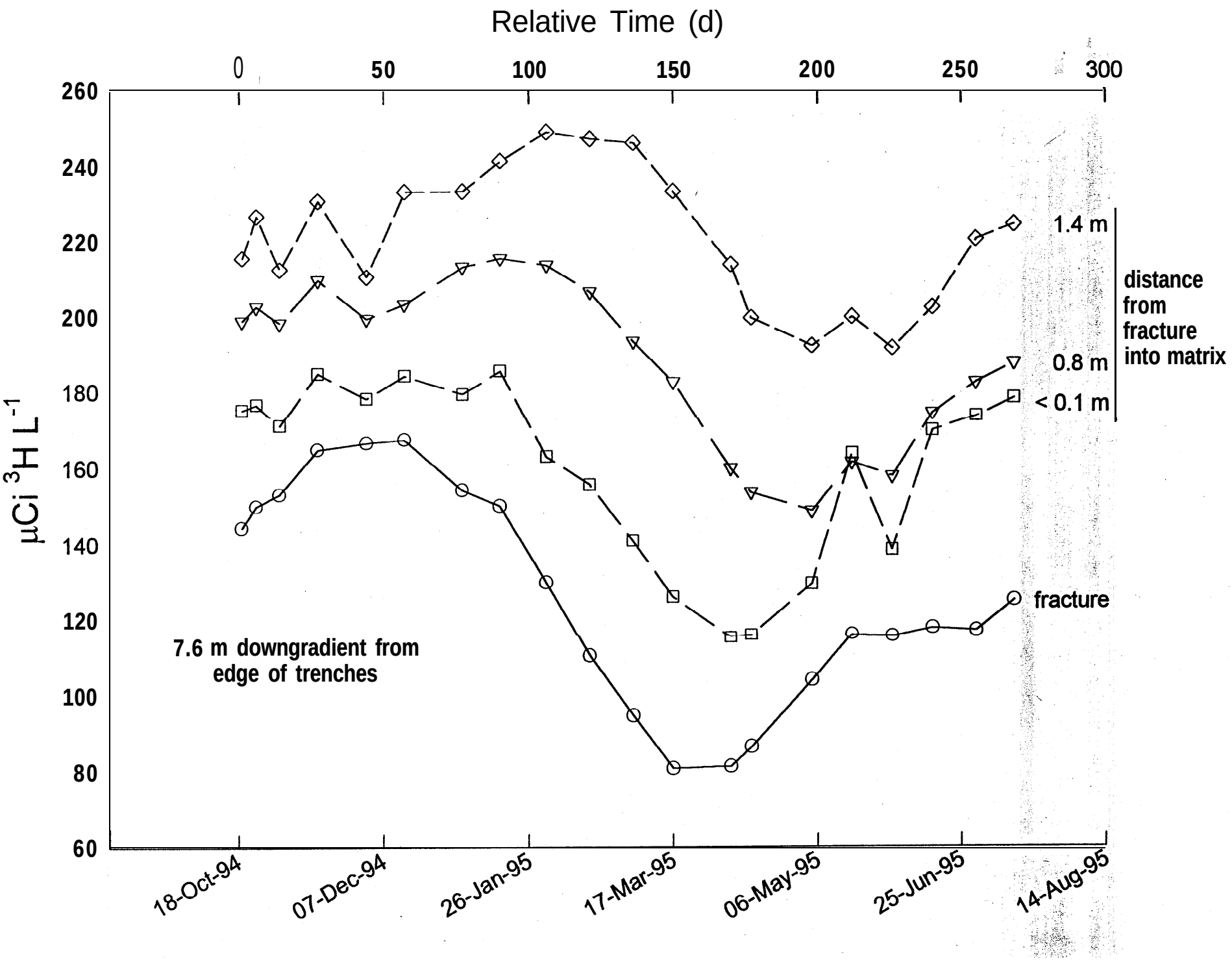
Relative Time (d)
0
50
100
150
200
250
300
260
240
220
200
180
160
140
120
100
80
60
μCi ^{3}H L^{-1}
1.4 m
0.8 m
< 0.1 m
distance from fracture into matrix
fracture
7.6 m downgradient from edge of trenches
18-Oct-94
07-Dec-94
26-Jan-95
17-Mar-95
06-May-95
25-Jun-95
14-Aug-95